Cell Genomics

Article

Multi-omics integration identifies cell-state-specific repression by PBRM1-PIAS1 cooperation

Graphical abstract

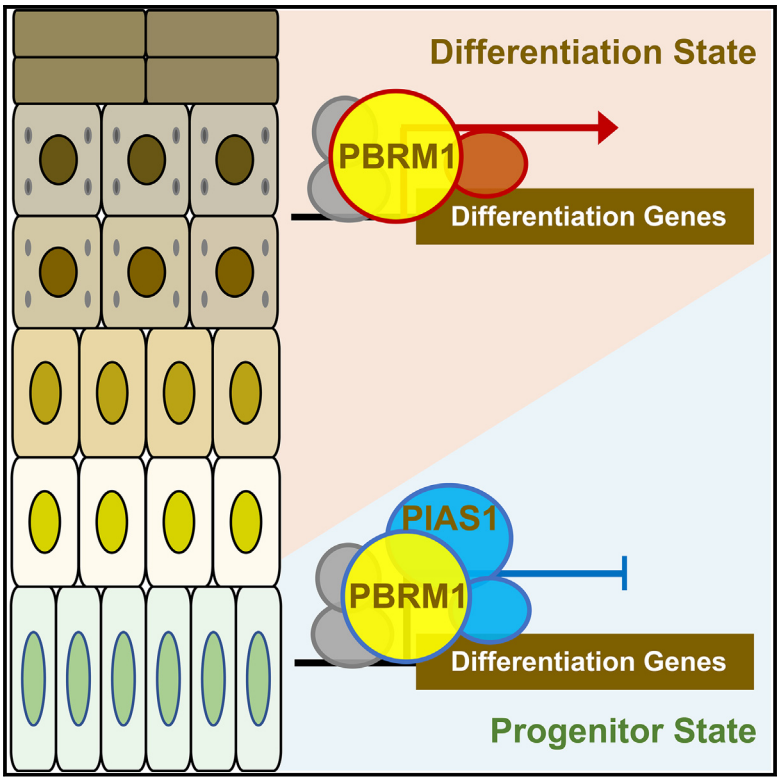

Highlights

- PBRM1 represses differentiation in progenitors but not in the differentiation state
- PBRM1's protein interactome, but not genomic binding, alters in cell-state switch
- PIAS1 and PBRM1 co-localize on chromatin in progenitors but not in differentiation
- SUMOylation contributes to PBRM1's repressive function in progenitor maintenance

Authors

Patric J. Ho, Junghun Kweon, Laura A. Blumensaadt, ..., Sarah M. Lloyd, Ziyou Ren, Xiaomin Bao

Correspondence

xiaomin.bao@northwestern.edu

In brief

Ho et al. demonstrate that PBRM1 switches from repressive to activating roles in differentiation gene regulation, as human skin epidermal cells transition from progenitor state to differentiation state. They identified that the changes in PBRM1's interacting proteins such as PIAS1, but not PBRM1's genomic binding, underlie this functional change.

Ho et al., 2024, Cell Genomics *4*, 100471
January 10, 2024
https://doi.org/10.1016/j.xgen.2023.100471

CellPress

Cell Genomics

CellPress
OPEN ACCESS

Article

Multi-omics integration identifies cell-state-specific repression by PBRM1-PIAS1 cooperation

Patric J. Ho,[1] Junghun Kweon,[1] Laura A. Blumensaadt,[1] Amy E. Neely,[1] Elizabeth Kalika,[1] Daniel B. Leon,[1] Sanghyon Oh,[1] Cooper W.P. Stringer,[1] Sarah M. Lloyd,[1] Ziyou Ren,[2] and Xiaomin Bao[1,2,3,4,*]

[1]Department of Molecular Biosciences, Northwestern University, Evanston, IL 60208, USA
[2]Department of Dermatology, Northwestern University, Chicago, IL 60611, USA
[3]Robert H. Lurie Comprehensive Cancer Center, Northwestern University, Chicago, IL 60611, USA
[4]Lead contact
*Correspondence: xiaomin.bao@northwestern.edu
https://doi.org/10.1016/j.xgen.2023.100471

SUMMARY

PBRM1 is frequently mutated in cancers of epithelial origin. How PBRM1 regulates normal epithelial homeostasis, prior to cancer initiation, remains unclear. Here, we show that PBRM1's gene regulatory roles differ drastically between cell states, leveraging human skin epithelium (epidermis) as a research platform. In progenitors, PBRM1 predominantly functions to repress terminal differentiation to sustain progenitors' regenerative potential; in the differentiation state, however, PBRM1 switches toward an activator. Between these two cell states, PBRM1 retains its genomic binding but associates with differential interacting proteins. Our targeted screen identified the E3 SUMO ligase PIAS1 as a key interactor. PIAS1 co-localizes with PBRM1 on chromatin to directly repress differentiation genes in progenitors, and PIAS1's chromatin binding drastically diminishes in differentiation. Furthermore, SUMOylation contributes to PBRM1's repressive function in progenitor maintenance. Thus, our findings highlight PBRM1's cell-state-specific regulatory roles influenced by its protein interactome despite its stable chromatin binding.

INTRODUCTION

Epithelial tissue, which lines the surfaces and cavities of all major organs, undergoes constant regeneration to compensate for wear and tear. Sustained tissue regeneration relies on the progenitors to continuously undergo self-renewal or differentiation, maintaining tissue architecture and function. Progenitor self-renewal requires the repression of terminal differentiation genes to maintain progenitors' regenerative potential. In the differentiation process, however, these genes must be activated to establish the epithelial barrier function. Dysregulation of differentiation gene expression underlies a spectrum of diseases, including cancer. The molecular mechanisms governing the repression or activation of terminal differentiation genes, in a specific cell state, remain incompletely understood.

Most life-threatening cancers originate from epithelial tissue. Recent cancer genomic sequencing studies identified BAF (SWI/SNF) as the most frequently mutated chromatin-associated complex in all human cancers.[1,2] Each BAF complex incorporates 10–13 regulatory subunits in addition to a single catalytic subunit.[3,4] While it is well recognized that the catalytic subunit repositions nucleosomes to activate gene expression,[5,6] how the regulatory subunits influence gene expression remains less clear. These regulatory subunits include PBRM1, a defining subunit of a specific BAF assembly termed PBAF. PBRM1 is recognized as the second most highly mutated gene in clear cell renal cell carcinoma (ccRCC).[7–11] Frequent PBRM1 mutations are also observed in several other types of epithelial cancer, including non-small cell lung cancer, intrahepatic cholangiocarcinoma, and mesothelioma.[12–14] In the context of gene regulation, PBRM1's roles as a co-activator have been reported in several cell types. In ccRCC cell lines with impaired PBRM1 function, re-introduction of wild-type PBRM1 was able to activate the terminal differentiation program.[15] For mesenchymal stem cells, PBRM1 is required for differentiating to the osteolineage, by activating the BMP/transforming growth factor β (TGF-β) receptor genes.[16] Intriguingly, in the context of DNA damage response, PBRM1 is required for the transcriptional silencing of the flanking regions near the damage sites.[17] Whether PBRM1's repressive function extends beyond the DNA damage response requires further investigation. It also remains unclear how PBRM1 influences gene expression in different cell states in normal epithelial homeostasis, before cancer arises.

The human skin epidermis, a type of stratified epithelium predominantly composed of keratinocytes, presents an accessible model for investigating gene regulatory mechanisms underlying epithelial homeostasis. Primary keratinocytes can be isolated and cultured from surgically discarded skin, retaining their regenerative potential to form full-thickness epidermal tissue. These cells can be cultured in either the progenitor state or

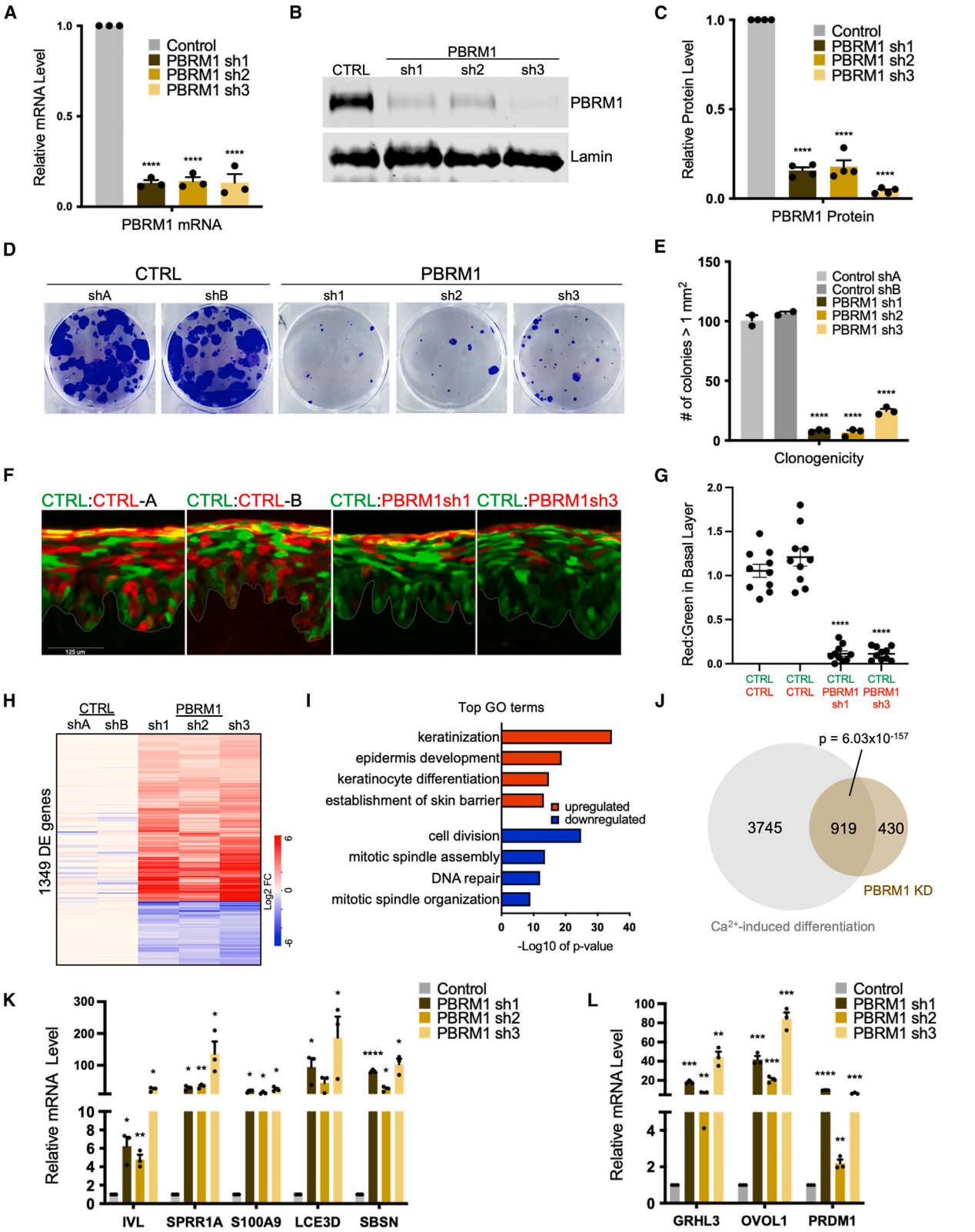

(legend on next page)

the differentiation state, providing sufficient cell numbers for the implementation of different "omics" approaches and for obtaining high-resolution results. Previous findings from us and others have highlighted BAF's crucial but complex roles in epidermal homeostasis. The catalytic subunits BRG1 and BRM are essential for activating terminal epidermal differentiation by maintaining the genome accessibility for the lineage-specific transcription factor p63.[5,18] The actin-like regulatory subunit ACTL6A (BAF53A), on the other hand, is required to repress terminal differentiation in progenitor maintenance.[19–21] How BAF associates with these two seemingly opposite functions remains unexplored. How other BAF subunits, such as PBRM1, influence gene expression in the progenitor-state versus differentiation-state keratinocytes also remains largely unclear.

In this study, we focused on characterizing PBRM1 in epidermal homeostasis. We found that PBRM1's gene regulatory roles differ drastically between the progenitor state and the differentiation state of keratinocytes. In the progenitor state, PBRM1 is required for repressing differentiation genes; in the differentiation state, PBRM1's repressive function diminishes, and PBRM1 becomes essential for activating a subset of differentiation genes. Between these two states, we identified drastic changes in PBRM1's protein interactome but not in its genomic binding profiles. Using a targeted RNAi screen focusing on the unique PBRM1-interacting proteins in the progenitor state, we identified the E3 SUMO ligase PIAS1 as a top candidate. PIAS1 binds to 56% of PBRM1 chromatin immunoprecipitation sequencing (ChIP-seq) peaks in the progenitor state but drastically reduces its chromatin binding in the differentiated state. RNA-seq further confirmed 896 differentially expressed genes directly co-regulated by both PBRM1 and PIAS1 in the progenitor state. We further identified that PBRM1 is associated with SUMOylation and that SUMOylation inhibition is sufficient to upregulate differentiation in the same pathway with PBRM1 knockdown. These findings indicate that PIAS1-PBRM1 cooperation is essential for repressing differentiation in epidermal progenitor maintenance. This study highlights the contributions of protein-protein interactions in influencing BAF's gene regulatory roles, despite its stable chromatin binding, in a cell-state-dependent manner to differentially control gene expression in tissue homeostasis.

RESULTS

PBRM1 loss de-represses differentiation in the progenitor state

To begin to investigate PBRM1's gene regulatory roles, we designed and screened multiple short hairpin RNAs (shRNAs) targeting PBRM1. Three independent shRNAs were validated at both the mRNA and protein levels, achieving over 80% knockdown efficiency (Figures 1A–1C). In the progenitor-state keratinocytes, PBRM1 knockdown drastically reduced clonogenicity when compared to the non-targeting control knockdowns (Figures 1D and 1E), suggesting that PBRM1 is essential for maintaining progenitor self-renewal. We subsequently performed a progenitor competition assay in epidermal tissue regeneration. In this assay, the same numbers of keratinocytes labeled with GFP or dsRed were mixed to regenerate epidermis in organotypic culture. dsRed-labeled keratinocytes co-expressing an shRNA targeting PBRM1, but not the non-targeting control shRNA, were outcompeted by GFP-labeled keratinocytes expressing the non-targeting control shRNA in the basal progenitor compartment of the regenerated epidermis (Figures 1F and 1G). Thus, the intact function of PBRM1 is essential for epidermal progenitor maintenance.

To determine how PBRM1 modulates the transcriptome in the progenitor state, we performed RNA-seq comparing keratinocytes expressing PBRM shRNAs or non-targeting control shRNAs. In total, 1,349 differentially expressed genes were identified (fold change $\geq$ 2, $p < 0.05$; Figure 1H; Table S1). Interestingly, the majority (72.9%) of these genes were upregulated, with their top Gene Ontology (GO) terms being associated with epidermal differentiation, such as "keratinization," "epidermal development," and "establishment of skin barrier." Only 27.1% differentially expressed genes were downregulated, and the GO terms of these genes were associated with cell proliferation (Figure 1I). These differentially expressed genes significantly overlap with the gene signature of calcium-induced

Figure 1. PBRM1 represses terminal differentiation in epidermal progenitor maintenance

(A) Bar graph showing the knockdown (KD) efficiency of PBRM1 with three independent shRNAs at the mRNA level using RT-qPCR (n = 3 biological replicates, ****$p < 0.0001$, two-tailed unpaired t test, data are represented as average ± standard error).

(B and C) Western blots and quantification showing the KD efficiency of the shRNAs targeting PBRM1 at the protein level (n = 4 biological replicates, ****$p < 0.0001$, two-tailed unpaired t test, data are represented as average ± standard error).

(D and E) Representative image of clonogenic assays comparing keratinocytes expressing PBRM1 shRNAs colonies versus control shRNAs. Colonies with diameter >1 mm^2 were quantified (****$p < 0.0001$, two-tailed unpaired t test, data are represented as average ± standard error).

(F and G) Representative images of epidermal tissue regenerated using 50% control shRNA labeled by GFP (green) and 50% PBRM1 shRNA or control shRNA labeled by dsRed (red). Dotted lines indicate the basement membrane. Scale bar: 125 μm. Representative images from 25 images per condition are shown. Quantification is of red:green ratio in the basal layer comparing tissue sections of CTRL/CTRL versus CTRL/PBRM1 sh (n = 10 images/condition, ****$p < 0.0001$, two-tailed unpaired t test, data are represented as average ± standard error).

(H) Heatmap showing the fold change of 1,349 differentially expressed genes from PBRM1 KD RNA-seq in the progenitor state (fold change $\geq$ 2, $p < 0.05$, DESeq2).

(I) Bar graph showing the top Gene Ontology (GO) terms of the genes differentially expressed from PBRM1 KD RNA-seq in the progenitor state.

(J) Venn diagram showing the overlap of significantly altered genes (fold change $\geq$ 2, $p < 0.05$, DESeq2) in PBRM1 KD keratinocytes and calcium-induced differentiated (DF) keratinocytes ($p = 6.03 \times 10^{-157}$, Fisher's exact test).

(K and L) Bar graphs showing the relative mRNA levels of epidermal differentiation markers and transcription factors between PBRM1 KD versus control shRNAs using RT-qPCR (n = 3 biological replicates, *$p < 0.05$, **$p < 0.01$, ***$p < 0.001$, ****$p < 0.0001$, two-tailed unpaired t test, data are represented as average ± standard error).

See also Figures S1 and S2 and Table S1.

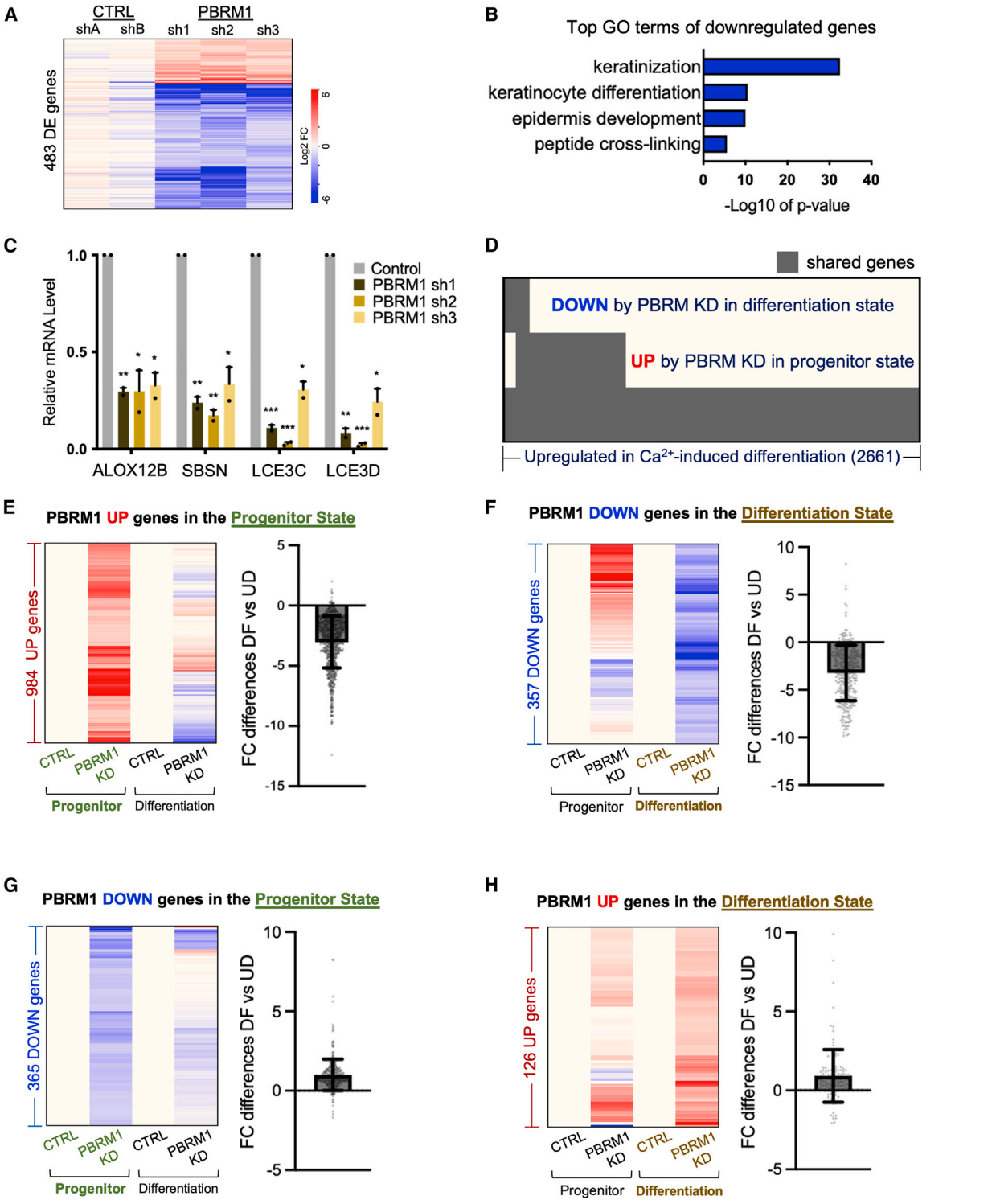

Figure 2. PBRM1's repressive function diminishes in the differentiation state

(A) Heatmap showing the fold change of 483 differentially expressed genes from PBRM1 KD RNA-seq in keratinocytes in the differentiation state (fold change ≥ 2, $p < 0.05$, DESeq2).

(B) Bar graph showing the top GO terms of significantly downregulated genes in PBRM1 KD RNA-seq.

(C) Bar graph showing the relative mRNA levels of epidermal differentiation markers and transcription factors from PBRM1 KD versus control in DF keratinocytes using RT-qPCR (n = 2 biological replicates, *$p < 0.05$, **$p < 0.01$, ***$p < 0.001$, two-tailed unpaired t test, data are represented as average ± standard error).

(legend continued on next page)

differentiation ($p = 6.03 \times 10^{-157}$, Fisher's exact test; Figures 1J, S1A, and S1B). Using RT-qPCR, we validated the upregulation of both epidermal differentiation marker genes (*IVL*, *SPRRIA*, *S100A9*, *LCE3D*, and *SBSN*) as well as differentiation-activating transcription factors (*GRHL3*, *OVOL1*, and *PRDM1*) with PBRM1 knockdown (Figures 1K and 1L). In addition, we confirmed that PBRM1 knockdown was not resulting in apoptosis (Figure S1C). Thus, these findings suggest that PBRM1 functions predominantly in repressing differentiation gene expression in progenitor maintenance.

Since PBRM1 is a defining subunit of the PBAF complex, we examined if PBRM1 knockdown influences the assembly and chromatin binding of other PBAF-specific subunits. Co-immunoprecipitation experiments using an ARID2 antibody showed that ARID2 retained its association with BRG1 and BRD7 in keratinocytes with PBRM1 knockdown, suggesting that the rest of PBAF complex can still assemble in this context (Figure S2A). To determine if the chromatin binding of other PBAF-specific subunits is altered with PBRM1 knockdown, we optimized the CUT&RUN technique for BRD7 and compared between keratinocytes with PBRM1 knockdown versus non-targeting control. To our surprise, PBRM1 knockdown using the three shRNAs consistently abolished BRD7 chromatin binding when compared to the two independent control shRNAs (Figures S2B–S2E). These results suggest that PBRM1, which features six bromodomains, is essential for chromatin binding but dispensable for the assembly of the partial PBAF complex in primary human keratinocytes.

PBRM1's repressive function diminishes in the differentiation state

Given PBRM1's repressive function in the progenitor state, we investigated if this repressive function is retained in the differentiated state. Keratinocytes expressing shRNAs targeting PBRM1 or non-targeting control shRNAs were seeded in the differentiation condition using the established protocol (full confluency for 4 days with 1.2 mM exogenous Ca^{2+}).[5,22,23] RNA-seq analysis identified a total of 483 genes that were differentially expressed between PBRM1 knockdown versus control conditions (fold change ≥ 2, $p < 0.05$, DEseq2; Table S2). Intriguingly, the majority (73.9%) of the differentially expressed genes in the differentiation state were downregulated by PBRM1 knockdown (Figure 2A), an opposite trend as compared to the observations from the progenitor state. The top GO terms of these downregulated genes were associated with epidermal terminal differentiation, such as "keratinization" and "keratinocyte differentiation" (Figure 2B). Only 126 genes were significantly upregulated without being associated with any significant GO terms ($p < 0.01$). Using RT-qPCR, we validated that representative differentiation marker genes (*SBSN*, *ALOX12B*, *LCE3D*, and *LCE3C*) were significantly downregulated with PBRM1 loss in the differentiation condition (Figure 2C). Thus, the cell-state switch involves drastic changes in differentiation gene expression regulated by PBRM1.

To clarify PBRM1's regulation of differentiation genes in the progenitor state versus the differentiation state, we compared the three groups of genes that were associated with terminal differentiation: (1) downregulated genes by PBRM1 knockdown in the differentiated state, (2) upregulated genes by PBRM1 knockdown in the progenitor state, and (3) upregulated genes in the Ca^{2+}-induced differentiation signature (Figure 2D). Of the genes that intersected with the Ca^{2+}-induced differentiation signature, only a subset of genes (55.5%, 91 genes) downregulated by PBRM1 knockdown (KD) in the differentiation state were shared with the upregulated genes by PBRM1 knockdown in the progenitor state. Furthermore, PBRM1 knockdown impacted about four times as many differentiation-related genes in the progenitor state than in the differentiation state. Most of the upregulated genes by PBRM1 KD in the progenitor state (87.1%, 615 genes) overlapped with the Ca^{2+}-induced differentiation signature without overlapping with the downregulated gene by PBRM1 KD in the differentiation state. These findings indicate that PBRM1 controls substantially distinct subsets of differentiation genes in the two cell states and that PBRM1 controls a broader spectrum of differentiation genes in the progenitor state than in the differentiation state.

We further compared the relative expression of individual genes with PBRM1 knockdown in the progenitor state versus the differentiation state. Among the 984 significantly upregulated genes by PBRM1 loss identified in the progenitor state, 97.8% of them showed reduced fold change in the differentiation state with an average reduction of 3.1 (log2) (Figure 2E), suggesting diminished repression and even gained activation of these individual genes in differentiation. Similarly, 92.2% of the 357 downregulated genes by PBRM1 loss in the differentiation state showed higher levels of relative fold change in the progenitor state, with an average reduction of 3.4 (log2) (Figure 2F), suggesting that most of them were less activated and even repressed in the progenitor state. In contrast, the downregulated genes in the progenitor state and the upregulated genes in the differentiated state showed only mild differences (log 2 fold change <1 in both cases) (Figures 2G and 2H). Taken together, the switch from the progenitor state to the differentiation state involves major changes in PBRM1's gene regulatory functions, especially for the target genes involved in differentiation.

PBRM1 directly represses differentiation genes in the progenitor state but retains its binding in the differentiation state

To determine how PBRM1 differentially regulates gene expression in the progenitor state versus the differentiation state, we compared PBRM1's chromatin binding using ChIP-seq. Among the total 17,527 PBRM1 ChIP-seq peaks we identified (MACS2,

(D) Gene set enrichment analysis (GSEA) comparing upregulated RNA-seq gene sets for calcium-induced DF keratinocytes, upregulated RNA-seq gene sets for PBRM1 KD in epidermal progenitors, and downregulated RNA-seq gene sets for PBRM1 KD in DF keratinocytes.
(E–H) Heatmaps comparing the relative expression in PBRM1 KD and control KD, between the progenitor state and the differentiation state, in the list of significantly upregulated or downregulated genes identified in the progenitor state or differentiation state with PBRM1 KD. The differences of the relative fold change for each gene, between the progenitor state and differentiation state, are indicated in the dot plots on the right.
See also Table S2.

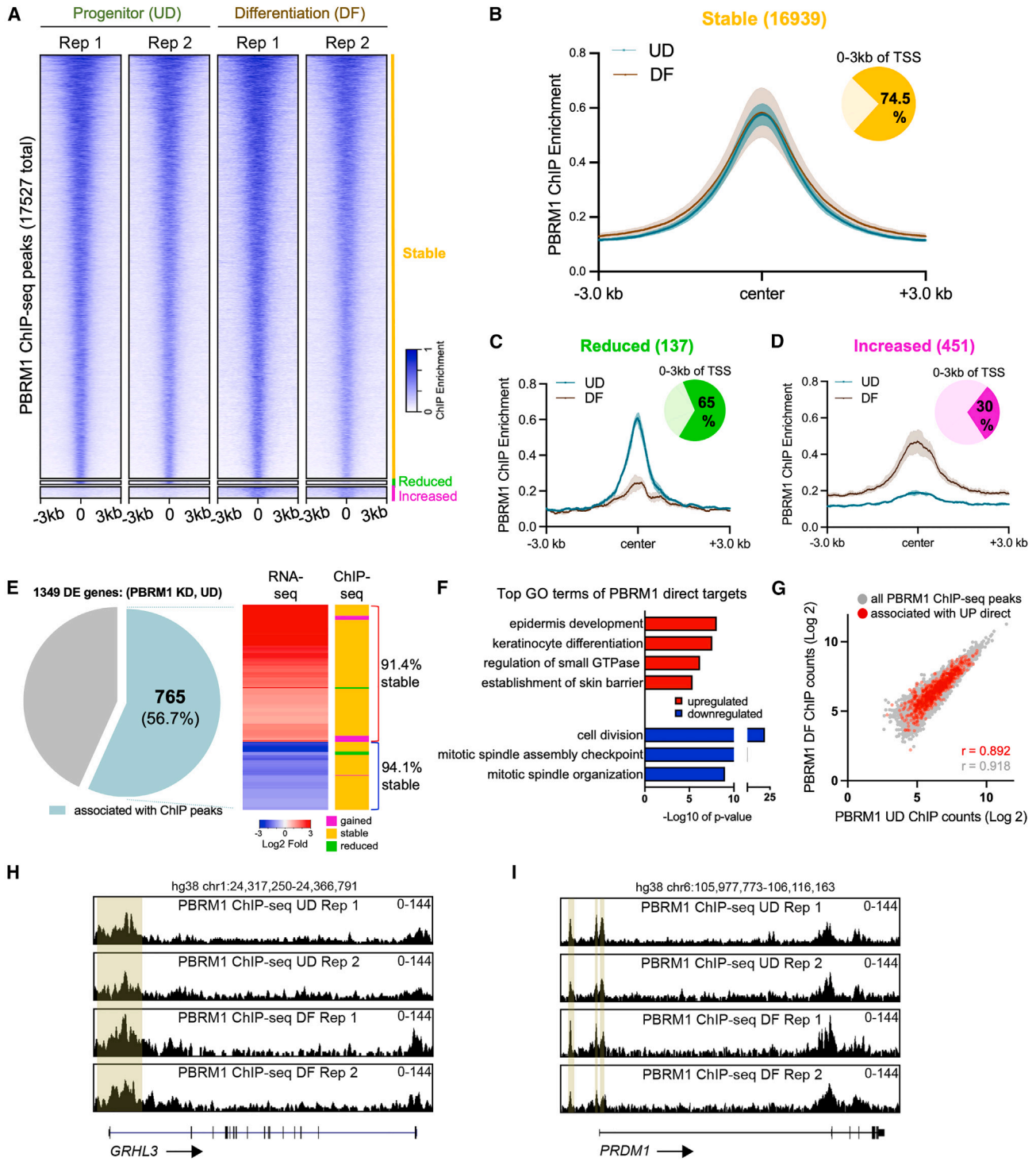

Figure 3. PBRM1 retains its genomic binding between the progenitor and differentiation states

(A) Summit-centered heatmaps comparing PBRM1 ChIP-seq enrichment between the progenitor state (UD) versus the differentiation state (DF). The 17,527 total peaks are divided into 3 groups ("stable," "reduced," and "increased") based on differential analysis of the peaks between UD and DF (fold change ≥ 2, $p < 0.05$, EdgeR).

(B–D) Average profile plots of PBRM1 ChIP-seq for the "stable," "reduced," and "increased" groups. Lines represent the average enrichment between the two PBRM1 ChIP-seq replicates in the progenitor state (dark green) or the differentiation state (dark brown). The shared areas indicate standard errors between the

(legend continued on next page)

broad peak, q < 0.001; Table S3), 96.6% of these peaks did not show significant changes in PBRM1 ChIP enrichment between the two states (fold change ≥ 2, p < 0.05, EdgeR). We termed these as "stable peaks." Only 137 (0.8%) peaks were significantly reduced and 451 (2.6%) peaks were significantly gained in the differentiation state. Most of the stable peaks (74.5%) and the reduced peaks (65%) were localized within 3 kb of the transcription start sites (TSSs) (Figures 3A–3D). To determine how PBRM1's chromatin binding influences gene expression, we assigned the ChIP-seq peaks to the genes associated with the nearest TSSs. Intersection of the ChIP-seq and RNA-seq data led to the identification of 765 direct targets in the progenitor state. 512 (67%) of these direct target genes were upregulated with PBRM1 knockdown, with GO terms related to "keratinocyte differentiation" and "epidermal development." The downregulated direct target genes (33%, 253 genes) were associated with the cell cycle. In particular, 94.1% of the downregulated direct targets (238 out of 253) and 91.4% of the upregulated direct targets (468 out of 512) were associated with stable PBRM1 ChIP peaks between the progenitor state and the differentiation state (Figures 3E and 3F). PBRM1 ChIP-seq enrichment, between the progenitor state and the differentiation state, also demonstrated high correlation in peaks associated with the upregulated and downregulated direct targets (Figures 3G and S3). These direct target genes associated with stable PBRM1 chromatin binding included the differentiation-activating transcription factors *PRDM1* and *GRHL3*, which are repressed by PBRM1 in the progenitor state but not in the differentiation state (Figures 3H and 3I). Therefore, the drastic changes of PBRM1's regulatory function on differentiation genes is not a result of altered PBRM1 chromatin binding.

Proteomic screen identified PIAS1-PBRM1 interaction enriched in the progenitor state

As PBRM1's chromatin binding between the two states did not explain its differential regulatory roles between the cell states, we subsequently investigated PBRM1's protein-protein interactions, leveraging the recently developed TurboID proximity labeling system.[24,25] We tagged PBRM1 at either its N terminus or C terminus using the TurboID tag fused with 3xHA and a nuclear localization sequence (NLS). The expression of TurboID with 3xHA and NLS by itself served as a negative control (Figure 4A). We expressed these constructs in both undifferentiated and differentiated keratinocytes, purified the biotinylated proteins, and submitted the gel bands for protein identification using mass spectrometry. Both C-terminal and N-terminal tagging identified the core subunits of the PBAF complex in both the progenitor state and the differentiation state. These included PBRM1 itself, SMARCC2 (BAF170), SMARCC1 (BAF155), ARID2, SMARCA4 (BRG1), SMARCA2 (BRM), and BRD7 (Figures S4A and S4B). To identify the differential PBRM1-interacting proteins, we calculated the relative enrichment ratio between the progenitor state and the differentiation state. The PBAF core subunits as well as the lineage-specific transcription factor p63 showed comparable enrichment in both cell states.

Interestingly, we identified a group of proteins that are detected only in the progenitor state but not in the differentiation state (Figures 4B and 4C). At the mRNA level, the genes encoding these progenitor-specific interacting proteins showed variable relative expression levels in differentiation (Figure S4C). To determine which of these proteins may cooperate with PBRM1 in repressing differentiation in the progenitor, we performed a targeted genetic screen. Two shRNAs were designed and validated for each of the top 8 most enriched PBRM1-interacting proteins. Knockdowns were performed in the progenitor state to evaluate the relative expression of representative differentiation genes (*OVOL1*, *SBSN*, *SPRR1A*, *GRHL3*, and *PRDM1*) using RT-qPCR. PIAS1 stood out as the top candidate, with two shRNAs consistently resulting in high upregulation of these differentiation marker genes and transcription activators (Figure 4D). Using co-immunoprecipitation, we further validated that the PIAS-PBRM1 interaction is significantly enriched in the progenitor state when compared to the differentiation state (Figures 4E and 4F). These findings suggest that PIAS1 may play a crucial role in cooperating with PBRM1 to repress differentiation in progenitor maintenance.

PIAS1 knockdown phenocopies PBRM1 knockdown in the progenitor state

Building on the substantial upregulation of representative differentiation marker genes in PIAS1 knockdown, we proceeded to functionally characterize PIAS1 knockdown in more detail in progenitor-state keratinocytes. The knockdown efficiency was validated at the protein level (Figures 5A and 5B). Similar to what was observed with PBRM1 knockdown, keratinocytes with PIAS1 knockdown exhibited drastically reduced clonogenicity when compared to the non-targeting controls (Figures 5C and 5D). In the progenitor competition assay, PIAS1 knockdown cells were also depleted from the basal progenitor compartment of the regenerated epidermal tissue (Figures 5E and 5F). These data indicate that PIAS1, similar to PBRM1, is essential for maintaining the regenerative capacity of epidermal progenitors.

biological replicates. In each group, the percentage of peaks within 3 kb from the nearest transcription start sites (TSSs) is represented in dark shade in the associated pie charts.

(E) Pie chart showing the subset of differentially expressed genes from PBRM1 KD RNA-seq in progenitors that are associated with PBRM1 ChIP-seq peaks. The relative expression of these genes in PBRM1 KD are shown in the red-blue heatmap, and the relative changes of PBRM1 ChIP-seq peaks between UD and DF (stable, gained, or reduced) are represented in the orange-magenta-green heatmap.

(F) Bar graph showing the top GO terms of the direct target genes, which are differentially expressed in PBRM1 KD RNA-seq in progenitors and are also associated with PBRM1 ChIP peaks.

(G) Scatterplot comparing PBRM1 ChIP enrichment in all the peaks between UD versus DF (gray, Pearson's coefficient r = 0.918), as well as the peaks associated with the upregulated direct target genes (red, Pearson's coefficient r = 0.892).

(H and I) Representative genome browser tracks showing the stable binding of PBRM1 near the promoter regions of representative transcriptional activators of epidermal terminal differentiation, such as *PRDM1* and *GRHL3*, in the progenitor and differentiation states. ChIP-seq peaks are highlighted in beige.

See also Figure S3 and Table S3.

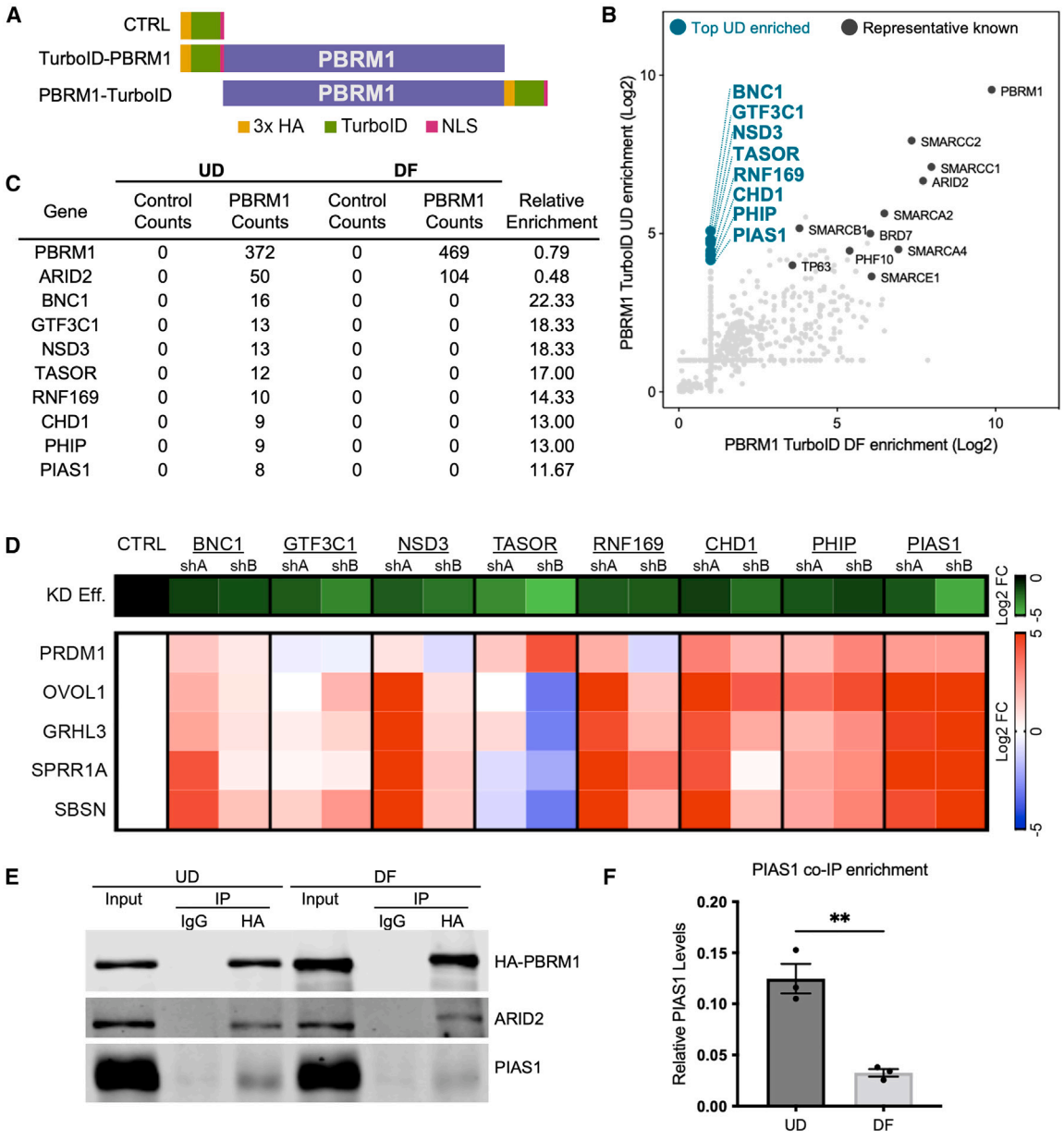

Gene	UD Control Counts	UD PBRM1 Counts	DF Control Counts	DF PBRM1 Counts	Relative Enrichment
PBRM1	0	372	0	469	0.79
ARID2	0	50	0	104	0.48
BNC1	0	16	0	0	22.33
GTF3C1	0	13	0	0	18.33
NSD3	0	13	0	0	18.33
TASOR	0	12	0	0	17.00
RNF169	0	10	0	0	14.33
CHD1	0	9	0	0	13.00
PHIP	0	9	0	0	13.00
PIAS1	0	8	0	0	11.67

Figure 4. Proximity labeling coupled with a targeted screen identified PIAS1-PBRM1 interaction in progenitors

(A) Schematic of the PBRM1 TurboID and control constructs used for proximity labeling to identify PBRM1-interacting proteins in UD and DF keratinocytes.

(B) Scatterplot showing the relative enrichment of proteins identified by PBRM1 TurboID in the progenitor state versus the differentiation state. Representative known interacting proteins, such as other PBAF subunits and p63, are labeled in dark gray. Top enriched PBRM1-interacting proteins in the progenitor state identified by TurboID are labeled in green.

(C) Table comparing the spectra counts of representative proteins identified from the TurboID experiments between the progenitor state versus the differentiation state.

(D) Heatmaps showing the shRNA screen among the top enriched PBRM1-interacting proteins identified in the progenitor state. The green-black heatmap shows the KD efficiency of the two independent shRNAs designed for each target gene. The red-blue heatmap shows the fold induction of differentiation markers genes with shRNA-mediated KD.

(E and F) Western blots and quantification of PIAS1 enrichment in HA-PBRM1 co-immunoprecipitation experiments comparing the progenitor state versus the differentiation state (n = 3 biological replicates, **p < 0.01, two-tailed unpaired t test, data are represented as average ± standard error).

See also Figure S4.

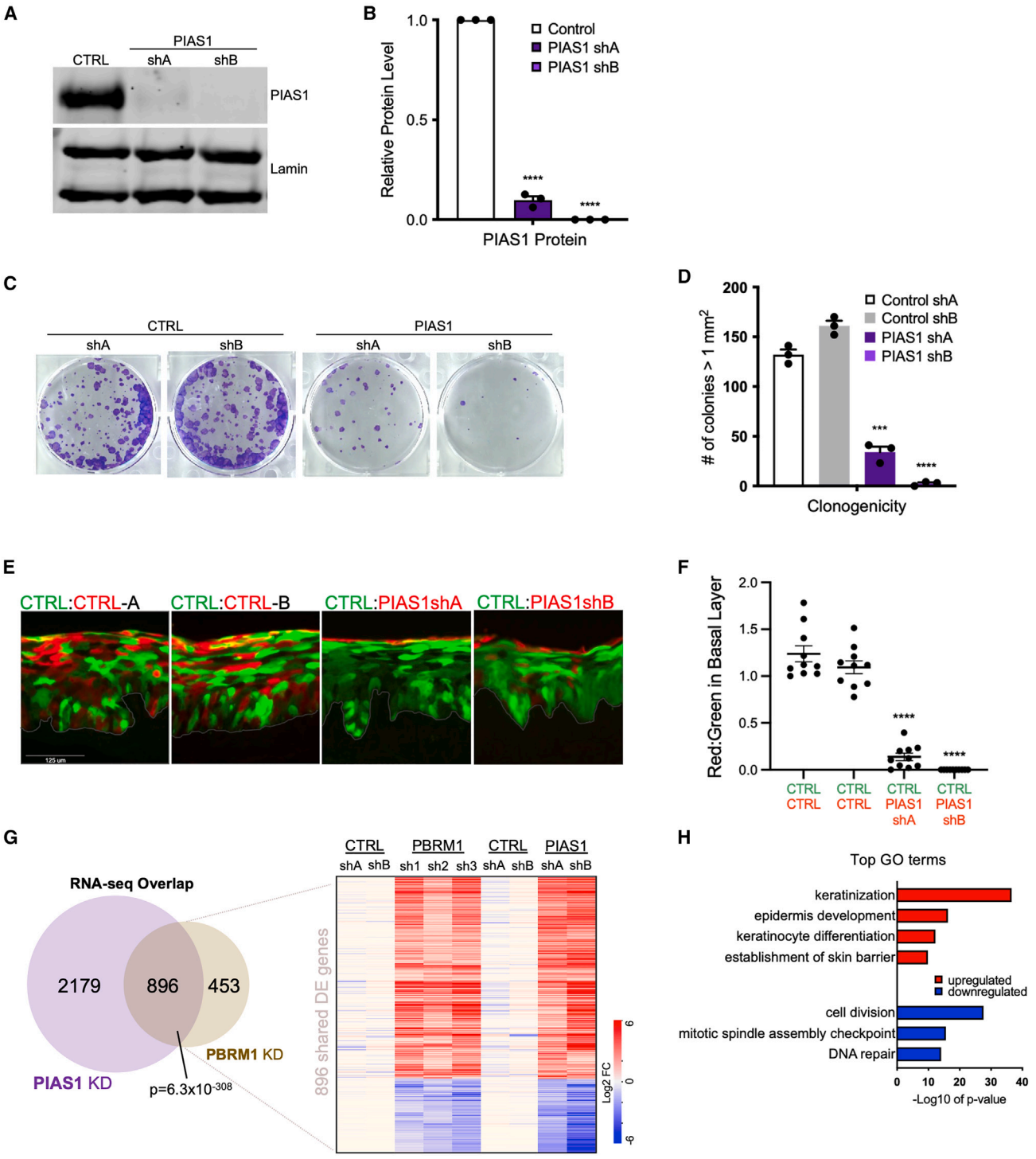

Figure 5. PIAS1 KD de-represses differentiation in the progenitor state

(A and B) Western blots and quantification showing the KD efficiency of PIAS1 using two independent shRNAs at the protein level (n = 3 biological replicates, ****p < 0.0001, two-tailed unpaired t test, data are represented as average ± standard error).

(C and D) Representative image of clonogenic assays comparing keratinocytes expressing PIAS1 shRNAs versus control shRNAs. Colonies with diameter >1 mm^2 were quantified (n = 3 technical replicates, ***p < 0.001, ****p < 0.0001, two-tailed unpaired t test, data are represented as average ± standard error).

(E and F) Representative image of epidermal tissue regenerated using 50% control shRNA labeled by GFP (green) and 50% PIAS1 shRNA or control shRNA labeled by dsRed mCherry (red). Scale bar: 125 μm. Quantification of red:green ratio in the basal layer comparing tissue sections of CTRL/CTRL versus CTRL/PIAS1 sh (n = 10 images per condition, ****p < 0.0001, two-tailed unpaired t test, data are represented as average ± standard error).

(legend continued on next page)

To identify how PIAS1 knockdown influences the transcriptome in the progenitors, beyond the selected markers initially tested using RT-qPCR in the initial screen, we performed RNA-seq. In total, we identified 3,075 genes that are differentially expressed with PIAS1 knockdown (fold change $\geq$ 2, $p < 0.05$, DEseq2; Table S4). Of those genes, 896 overlapped with the differentially expressed genes from PBRM1 knockdown in the progenitor state ($p = 6.3 \times 10^{-308}$, Fisher's exact test). In particular, these 896 genes accounted for 66.4% of total differentially expressed genes with PBRM1 knockdown and were altered in the same up- or downregulated direction by PBRM1 knockdown and PIAS1 knockdown. The majority (73.2%) of these PIAS1-PBRM1 overlapping genes were upregulated, and the top GO terms of these genes were associated with epidermal differentiation. The downregulated overlapping genes were associated with the cell cycle (Figures 5G and 5H). These findings suggest that PIAS1 and PBRM1 work together to regulate common target genes in progenitor maintenance, especially to repress differentiation gene expression.

Given the high degree of target gene overlap between PBRM1 and PIAS1 in the progenitor state, we further investigated how PIAS1 knockdown influenced gene expression in the differentiation state. PIAS1 knockdown in the differentiation state led to significant changes of 1,101 genes (Table S5). In contrast to PBRM1 knockdown in the differentiation state, which primarily impaired genes associated with terminal differentiation, these differentially expressed genes were associated with impaired cell division and growth (Figures S5A and S5B). Among all these 1,101 differentially expressed genes with PIAS1 knockdown, only 74 of these overlapped with PBRM1 knockdown, and these genes were not related to epidermal differentiation (Figures S5C–S5E). A juxtaposed comparison of these two datasets further indicated that the differentially expressed genes from PBRM1 knockdown were not recapitulated by PIAS1 knockdown in the differentiation state (Figure S5F). Thus, the gene expression changes with PIAS1 knockdown support its cooperation with PBRM1 in the progenitor state but not in the differentiation state.

PIAS1 co-localizes with PBRM1 near the TSSs to repress differentiation in the progenitor state

To determine how PIAS1 cooperates PBRM1 in gene regulation, we profiled PIAS1's chromatin-binding sites using ChIP-seq in the progenitor state and the differentiation state. In contrast to the stable binding of PBRM1, we observed that PIAS1's genomic binding diminished in the differentiation state. Among the total 20,083 peaks identified, 19,856 (98.7%) showed significant reduction of ChIP enrichment ($p < 0.05$, fold change $\geq$ 2, EdgeR) in the differentiation state (Figures 6A–6C; Table S6). In total, these PIAS1 ChIP-seq peaks overlapped with 55.5% PBRM1 ChIP-seq peaks (Figure 6D), and PIAS1 ChIP-seq peaks also exhibited higher enrichment in distal intergenic regions as compared to PBRM1 ChIP-seq peaks (Figure S6A). The PIAS1-unique peaks were primarily localized away from the TSSs, with enriched motifs related to the AP1 and p53 family transcription factors (Figure S6B). In contrast, the overlapping peaks between PIAS1 and PBRM1 were predominantly (85.4%) located within 3 kb of their nearest TSSs, suggesting that PIAS1, in association with PBRM1, may play distinct roles in gene regulation in association with PBRM1. By assigning the overlapping ChIP-seq peaks to the nearest TSSs, we identified that 369 out of the total 896 genes downstream to PBRM1 and PIAS1 were associated with their direct ChIP-seq binding (Figure 6E). Furthermore, 92.1% of these direct targets (340 out of 369) were associated with stable PBRM1 binding but with reduction of PIAS1 binding in differentiation. These direct target genes were related to cell cycle and keratinocyte differentiation processes (Figure S6C). In particular, these shared direct targets included transcription factors that are upregulated during the differentiation process to drive epidermal barrier function, including both *GRHL3* and *PRDM1* (Figures 6F and 6G). Thus, PBRM1 and PIAS1 co-bind near the TSSs to repress terminal differentiation in progenitor maintenance.

Given the PBRM-PIAS1 association in chromatin binding and gene regulation in the progenitor state, but not in the differentiation state, we further investigated their relative expression in these two cell states (Figure S7). Although PIAS1's expression was significantly upregulated at the mRNA level in differentiation, its protein expression showed significant reduction, with an average of 46% remaining levels in differentiation. This downregulation of PIAS1 was consistently observed in human tissue sections, with PIAS1 immunofluorescence staining signals being enriched in the basal progenitor layer and reduced in the differentiated epidermal layers immediately above the basal progenitor layer. PBRM1 also showed modest reduction at both the mRNA and the protein levels in keratinocyte differentiation. Thus, PIAS1's downregulation in keratinocyte differentiation supports its association with PBRM1 in the progenitor-state keratinocytes, though additional factors are likely involved in this cell-state-specific interaction.

The repressive function of PBRM1 involves SUMOylation

Since PIAS1 is an E3 SUMO ligase, and given its cooperation in gene regulation with PBRM1 in progenitor maintenance, we asked if PBRM1 is associated with SUMOylation. Leveraging proximity ligation assay (PLA), we detected strong signals between SUMO (SUMO1 or SUMO2/3/4) and the HA-tagged PBRM1 (Figure 7A), suggesting that PBRM1 is in proximity with SUMOylation. To determine if SUMOylation is involved in repressing differentiation in the progenitor state, we leveraged the SUMO inhibitor ML792 that targets the SUMO-activating enzyme (SAE).[26] Keratinocytes treated with ML792 resulted in the upregulation of differentiation genes in a time- and dose-dependent manner (Figures 7B and 7C), suggesting that SUMOylation is

(G) Venn diagram comparing the differentially expressed genes with PIAS1 KD or PBRM1 KD in RNA-seq in the progenitor state. Heatmap shows the relative fold change of the 896 overlapping genes in PIAS1 KD or PBRM1 KD RNA-seq in the progenitor state (fold change $\geq$ 2, $p < 0.05$, DESeq2).
(H) Bar graph showing the top GO terms of the overlapping genes differentially altered in PIAS1 KD RNA-seq and PBRM1 KD RNA-seq in the progenitor state.
See also Figure S5 and Tables S4 and S5.

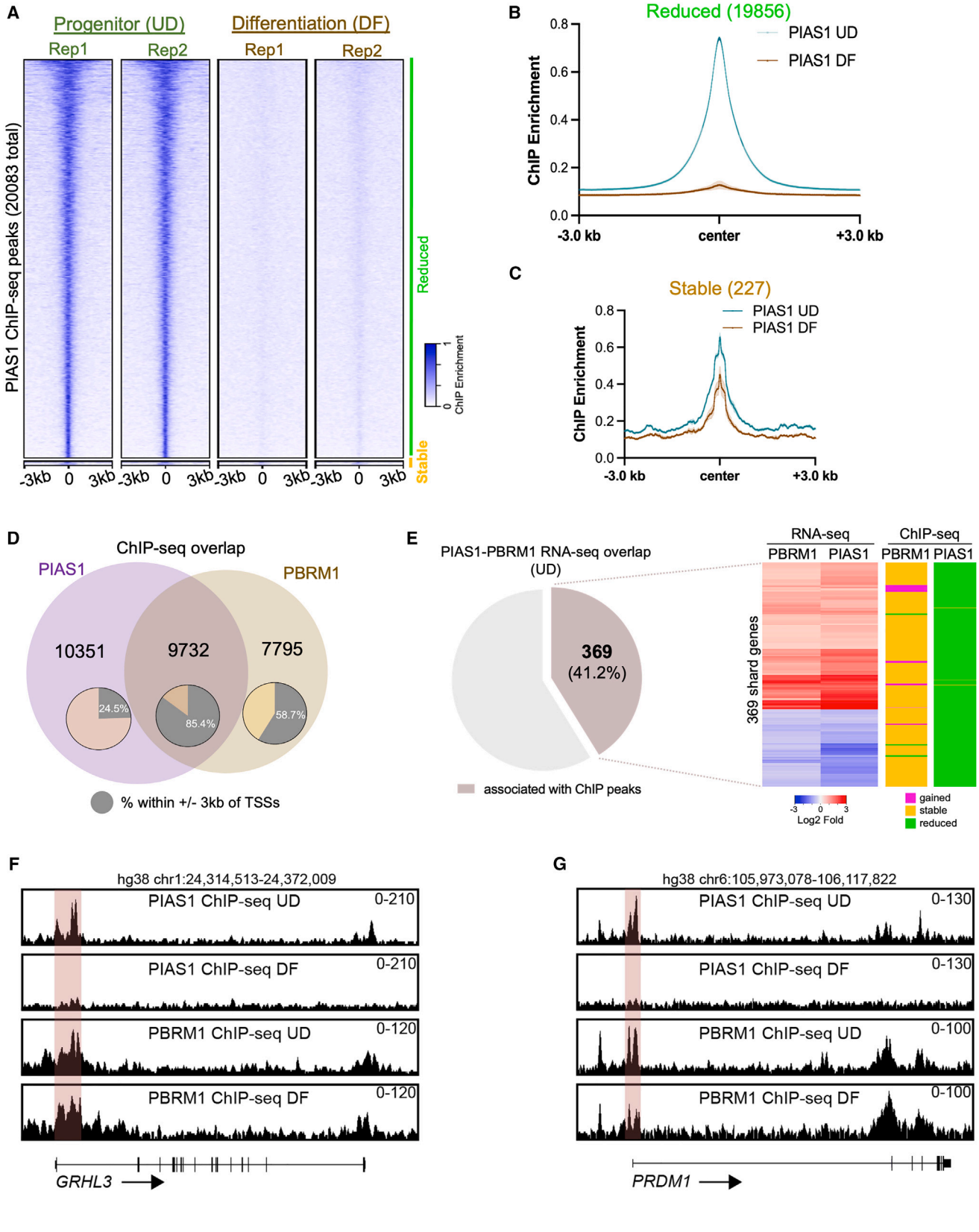

(legend on next page)

involved in repressing differentiation. Interestingly, SUMOylation inhibition did not further elevate the induction of differentiation from PBRM1 knockdown (Figures 7D and 7E), suggesting that SUMOylation and PBRM1 function in the same pathway to repress differentiation in the progenitor state.

DISCUSSION

Our findings highlight the cell-state-specific gene regulation by PBRM1, even when its chromatin binding remains stable between the different cell states. By integrating proteomics and genomics, we uncovered that the differential protein-protein interactions underlie the differential gene regulatory roles of PBRM1. Our findings further identified the PBRM1-PIAS1 interaction in repressing differentiation in the progenitor state but not in the differentiation state. Although cell-state-specific gene regulation by the BAF complex has been recognized, such as in the context of T cell activation and exhaustion,[27] the molecular mechanisms underlying this observation remained unclear, partially due to limitations in obtaining sufficient cell numbers for in-depth proteomic profiling in many types of primary cells. The expandability of primary human keratinocytes provides an advantage in integrating proteomics, together with genomics and human tissue genetics, to investigate gene regulatory mechanisms controlled by BAF in different cell states.

In the differentiation state, our findings agree with several previous studies implicating PBRM1 functions as a co-activator in promoting differentiation, such as in osteolineage differentiation, kidney proximal tube differentiation, heart chamber maturation, and T cell activation.[15,16,28,29] However, in the progenitor-state keratinocytes, we uncovered that PBRM1 predominantly functions in repressing differentiation, and this repressive function influences a broader spectrum of target genes than the genes modulated by PBRM1's activating function. Our findings indicate that PBRM1's role in transcriptional repression extends beyond the DNA damage response.[17] These observations suggest a possibility that shared gene regulatory mechanisms could be employed in both DNA damage response (silencing of the flanking regions near the damaged sites) and progenitor maintenance (repressing terminal differentiation genes).

This study links PBRM1's repressive function to the E3 SUMO ligase PIAS1. In contrast to PBRM1, PIAS1's role as a repressor has been reported in multiple contexts, including the repression of differentiation in natural regulatory T cells and hematopoietic stem cells.[30,31] As an E3 SUMO ligase, multiple PIAS1 substrates have been identified in the context of transcriptional regulation, including the androgen receptor (AR), STAT1, MYC, p53, and MAML1.[32–36] A recent study further identified more than 500 potential PIAS1 substrates using quantitative SUMO profiling.[37] Consistent with PIAS1's roles as a repressor, we found that PIAS1 directly binds near the TSSs of differentiation-activating transcription factors and differentiation effectors to repress their expression. We also uncovered that PBRM1 is associated with SUMOylation and that SUMOylation inhibition also de-represses keratinocyte differentiation. Furthermore, we found that this PBRM1-PIAS1 interaction is enriched in the progenitor state and that PIAS1 chromatin binding drastically reduces in the differentiation state. These observations suggest that PIAS1 as well as its SUMO ligase activity contribute to PBRM1's role as a repressor. SUMOylation has been previously linked to the recruitment of transcriptional repressors such as the histone deacetylases (HDACs).[38,39] In keratinocytes, HDACs play essential roles in repressing differentiation gene expression in progenitor maintenance,[40,41] and the acetyltransferase p300 is involved in activating terminal differentiation in cooperation with the BAF complex.[5] Therefore, we speculate that PBRM1's association with SUMOylation could facilitate the recruitment of HDAC to the differentiation gene promoters in undifferentiated keratinocytes to repress differentiation, whereas in the differentiation state, the dissociation between PIAS1 and PBRM1 may promote the association between p300 and PBAF to activate keratinocyte terminal differentiation.

Using TurboID coupled with a targeted RNAi screen, we identified PBRM1-interacting proteins unique to the progenitor state or the differentiation state. Although PBRM1's interacting proteins have been investigated using IP mass spectrometry in 293T cells and ACHN cells, only limited interactors were identified.[15] None of the top candidates we identified in progenitor-state keratinocytes were reported in that previous study. PIAS1 stood out from our targeted screen, with two shRNAs both consistently inducing high levels of representative differentiation marker expression; however, these findings do not exclude the impact from other PBRM1-interacting proteins in repressing differentiation. For example, the two shRNAs targeting PHIP also consistently upregulated differentiation marker gene expression,

Figure 6. PIAS1 co-localizes with PBRM1 to directly repress differentiation genes in progenitors

(A) Summit-centered heatmap comparing PIAS1 ChIP-seq enrichment in the progenitor state (UD) and the differentiation state (DF). Among the 20,083 total PIAS1 ChIP-seq peaks, two groups ("stable" and "reduced") were identified from differential analysis (fold change ≥ 2, $p < 0.05$, EdgeR).

(B and C) Average profile plots comparing PIAS1 ChIP-seq enrichment in progenitors (UD) and DF keratinocytes in the two groups. Dark lines represent the average enrichment between the two PIAS1 ChIP-seq replicates in the progenitor state (dark green) or the differentiation state (dark brown). The shared areas indicate standard errors between the replicates.

(D) Venn diagram showing the overlap of PIAS1 total ChIP-seq peaks and PBRM1 total ChIP-seq peaks, with pie charts showing the percentage of peaks within 3 kb of the nearest TSSs in each category.

(E) Pie chart showing the percentage of differentially expressed genes identified in both PIAS1 and PBRM1 KD RNA-seq in progenitors that associate with ChIP-seq peaks of both PIAS1 and PBRM1. These are identified as "direct target genes" of PIAS1 and PBRM1. The red-blue heatmap shows the relative expression of these direct target genes in RNA-seq data with PIAS1 KD or PBRM1 KD. The orange-magenta-green heatmap shows the relative changes of PIAS1 or PBRM1 ChIP-seq peaks between UD and DF (stable, gained, or reduced).

(F and G) Representative genome browser tracks showing the co-localization of PIAS1 and PBRM1 near the TSSs of representative differentiation-activating transcription factors such as *GRHL3* and *PRDM1*. ChIP-seq peak regions are highlighted in red.

See also Figures S6 and S7 and Table S6.

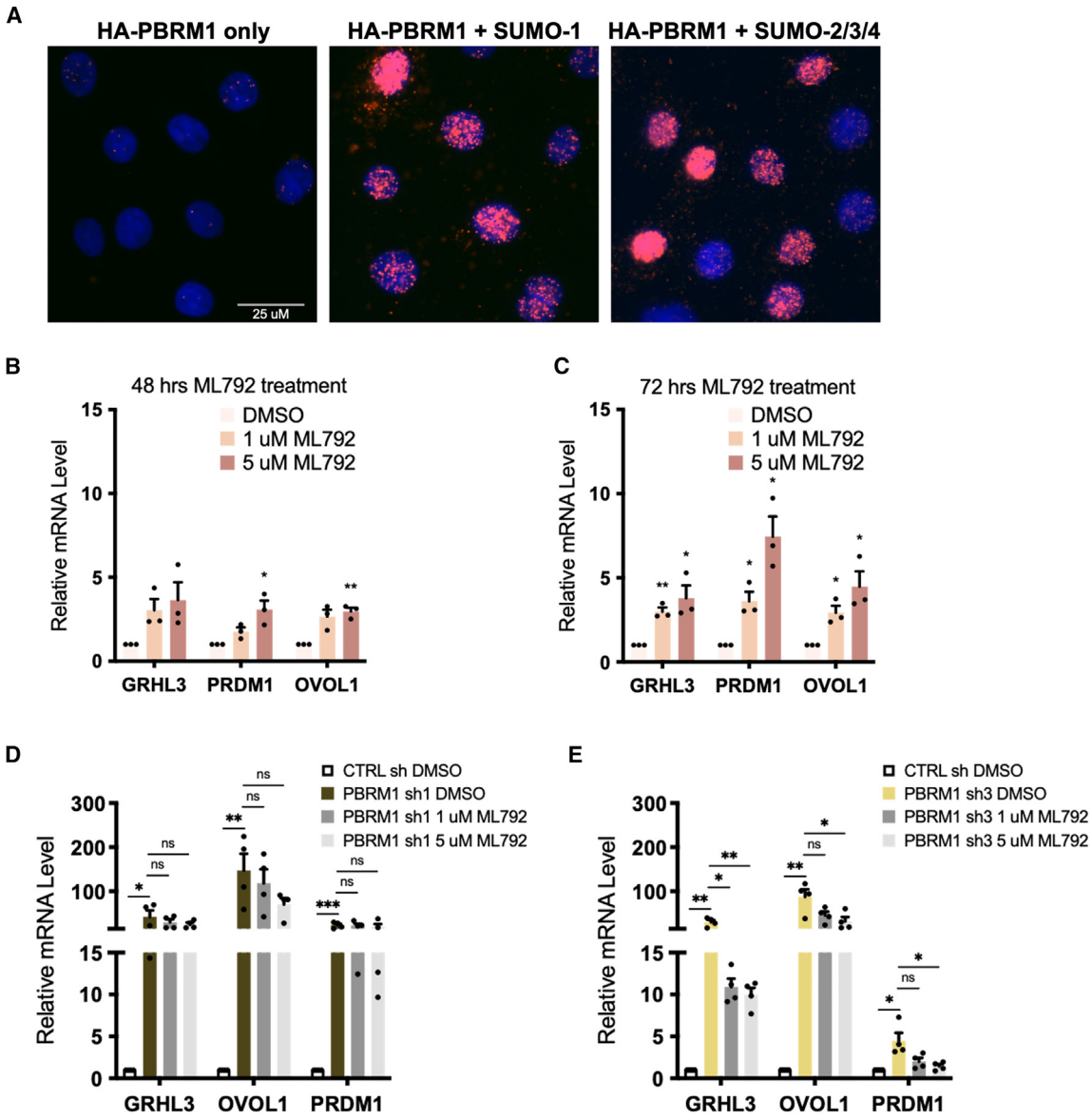

Figure 7. PBRM1's repressive function in progenitors involves SUMOylation

(A) Representative images of proximity ligation assay (PLA) using antibodies recognizing HA-PBRM1 (HA) or SUMOylation (SUMO-1 or SUMO-2/3/4). The nuclei are stained with Hoechst 33342, and the PLA signals are shown as red dots. Scale bar: 25 μm.

(B and C) Bar graphs showing the relative expression of representative PIAS1-PBRM1 direct target genes (*GRHL3*, *OVOL1*, *PRDM1*), with 2 different doses and time points of the SUMOylation inhibitor ML792, in progenitor-state keratinocytes (n = 3 biological replicates, *p < 0.05, **p < 0.01, two-tailed unpaired t test, data are represented as average ± standard error).

(D and E) Bar graphs comparing the relative expression of representative PIAS1-PBRM1 direct target genes (*GRHL3*, *OVOL1*, *PRDM1*), in PBRM1 KD with or without the addition of ML792, in progenitor-state keratinocytes (n = 4 biological replicates, *p < 0.05, **p < 0.01, ***p < 0.001, two-tailed unpaired t test, data are represented as average ± standard error).

although the relative fold change was not as high as what was observed with PIAS1 knockdown. Similarly, CHD1 knockdown also led to the upregulation of multiple differentiation markers. These findings suggest that PBRM1's repressive function is more likely to be a result of multiple protein-protein interactions, with PIAS1 being one of them. Future studies will be necessary to clarify how these PBRM1-interacting proteins cooperate with each other to establish the repressive function of differentiation genes in progenitor maintenance.

We found that PBRM1 knockdown diminished the chromatin binding of another PBAF-specific subunit, BRD7, without impairing its association with ARID2 and BRG1. These findings are consistent with the previous finding that PBRM1 is the last subunit to be integrated into the PBAF complex.[42] However, a recent

paper using a ccRCC cell line identified redistribution of other PBAF-specific subunits from the promoters to enhancers with PBRM1 loss.[43] The differences in chromatin binding of other PBAF subunits observed in this study can be explained by several potential reasons. First, the knockdown experiment of PBRM1 in primary human keratinocytes can be completed within several days, while the ccRCC cancer cells have been adapted to PBRM1 depletion for a much longer time period. It is possible that the cancer cells have evolved unique mechanisms to recruit the partial PBAF complex to chromatin during this long-term adaptation process. Second, ccRCC cancer cells have accumulated multiple alterations in gene regulation as compared to the primary human keratinocytes isolated from normal skin. These additional mutations may facilitate the recruitment of other PBAF subunits to chromatin. In addition, it is also possible that the chromatin-binding mechanisms of other PBAF subunits could be different between skin epidermal cells versus renal epithelial cells. Future work comparing the normal and cancer cells between these two tissue types can help to clarify the mechanistic details underlying the differences in chromatin-binding patterns.

Taken together, our findings highlight the plasticity of PBRM1's gene regulatory roles in different cell states. Without substantial alterations in its chromatin binding, PBRM1 switches from a predominantly repressive function to an activating function in the process of epithelial progenitor differentiation. Findings from this study suggest that altered protein interactions could be a mechanism underlying the functional changes. Further work elucidating how PBRM1 differentially interacts with additional unique subsets of interacting proteins, and whether PBRM1 mutations identified from cancer alter these specific interactions, will advance our understanding of PBAF's roles in normal tissue homeostasis and how different BAF mutations influence carcinogenesis.

Limitations of the study

Integrating genomics and proteomics, we identified 200 PBRM1-interacting proteins in the progenitor state or the differentiation state, though we elected to focus on the detailed characterization of PBRM1 and PIAS1 in this study. Other PBRM1-interacting proteins are likely to also influence PBRM1's functionality in gene regulation and will be characterized in detail in future studies. Although we used both the N-terminal and C-terminal tagging strategy to maximize the capture of its interacting proteins, the TurboID method is limited by the biotinylation radius (10–15 nm) and the availability of lysine residues on the surface.[44,45] Therefore, it is possible that this strategy might not have uncovered the entire PBAF interactome in the two states examined in this study. We also acknowledge the fact that different epithelial cell types have their own uniquely expressed proteins. This study is also limited to examining PBAF-interacting proteins in the progenitor state versus one time point in the differentiation time course (day 4). The process of keratinocyte differentiation typically takes 6 days. Therefore, day 4 differentiation represents a mid-to-late time point. While describing the binary switch between these two time points, it is possible that additional PBRM1 interactions occur between the time points as intermediate states between the transition. In addition, it is likely that the differentiation process in three-dimensional epidermal tissue may have unique features that were not fully recapitulated by this calcium-induced differentiation process in cultured primary human keratinocytes.

STAR★METHODS

Detailed methods are provided in the online version of this paper and include the following:

- KEY RESOURCES TABLE
- RESOURCE AVAILABILITY
  - Lead contact
  - Materials availability
  - Data and code availability
- EXPERIMENTAL MODEL AND SUBJECT DETAILS
  - Primary human keratinocyte isolation and culture
- METHOD DETAILS
  - Plasmid construction
  - Progenitor competition assay in epidermal tissue regeneration
  - Gene transfer and expression in keratinocytes
  - Inhibitor treatments
  - Clonogenicity assay
  - Apoptosis assay
  - Tissue immunofluorescence
  - RT-qPCR
  - Western blotting
  - Co-immunoprecipitation
  - Proximity ligation assay
  - PBRM1 TurboID and mass spectrometry
  - RNA-seq
  - ChIP-seq
  - CUT&RUN
- QUANTIFICATION AND STATISTICAL ANALYSIS
  - Organotypic culture tissue regeneration analysis
  - Colony formation assay analysis
  - RT-qPCR expression analysis
  - RNA-seq data analysis
  - ChIP-seq and CUT&RUN data analysis
  - TurboID proteomic data analysis

SUPPLEMENTAL INFORMATION

Supplemental information can be found online at https://doi.org/10.1016/j.xgen.2023.100471.

ACKNOWLEDGMENTS

We would like to thank the Skin Biology and Disease Resource-Based Center (SBDRC, P30AR075049) at Northwestern University for providing human skin tissues, cells, and media related to this study. We are grateful for the NUSeq and Proteomics core facilities at Northwestern University for supporting the generation of genomic and proteomic data. We would like to thank other members of the Bao Lab for the support and discussions. This study is supported by the following awards to X.B.: NIH R00/K99 (R00AR065480), NIH R01 (AR075015), American Cancer Society Research Scholar Grant (RSG-21-018-01-DDC), and the Searle Leadership Fund. In addition, this study is supported by the Carcinogenesis T32 Training Grant (T32CA009560) and Biotech Training Grant to support P.J.H. as a predoctoral trainee.

AUTHOR CONTRIBUTIONS

X.B. and P.J.H. designed this study, interpreted the data, and wrote the manuscript. P.J.H., J.K., L.A.B., A.E.N., D.B.L., S.O., E.K., C.W.P.S., and X.B. performed the experiments in this study. P.J.H., Z.R., S.M.L., and X.B. performed data analyses for this study.

DECLARATION OF INTERESTS

The authors declare no competing interests.

Received: May 6, 2023
Revised: October 24, 2023
Accepted: November 30, 2023
Published: January 2, 2024

REFERENCES

1. Kadoch, C., and Crabtree, G.R. (2015). Mammalian SWI/SNF chromatin remodeling complexes and cancer: Mechanistic insights gained from human genomics. Sci. Adv. *1*, e1500447.
2. Kadoch, C., Hargreaves, D.C., Hodges, C., Elias, L., Ho, L., Ranish, J., and Crabtree, G.R. (2013). Proteomic and bioinformatic analysis of mammalian SWI/SNF complexes identifies extensive roles in human malignancy. Nat. Genet. *45*, 592–601.
3. Wu, J.I., Lessard, J., and Crabtree, G.R. (2009). Understanding the words of chromatin regulation. Cell *136*, 200–206.
4. Ho, P.J., Lloyd, S.M., and Bao, X. (2019). Unwinding chromatin at the right places: how BAF is targeted to specific genomic locations during development. Development *146*, dev178780.
5. Bao, X., Rubin, A.J., Qu, K., Zhang, J., Giresi, P.G., Chang, H.Y., and Khavari, P.A. (2015). A novel ATAC-seq approach reveals lineage-specific reinforcement of the open chromatin landscape via cooperation between BAF and p63. Genome Biol. *16*, 284.
6. Morris, S. a, Baek, S., Sung, M.-H., John, S., Wiench, M., Johnson, T. a, Schiltz, R.L., and Hager, G.L. (2014). Overlapping chromatin-remodeling systems collaborate genome wide at dynamic chromatin transitions. Nat. Struct. Mol. Biol. *21*, 73–81.
7. Voss, M.H., Reising, A., Cheng, Y., Patel, P., Marker, M., Kuo, F., Chan, T.A., Choueiri, T.K., Hsieh, J.J., Hakimi, A.A., and Motzer, R.J. (2018). Genomically annotated risk model for advanced renal-cell carcinoma: a retrospective cohort study. Lancet Oncol. *19*, 1688–1698.
8. Nargund, A.M., Pham, C.G., Dong, Y., Wang, P.I., Osmangeyoglu, H.U., Xie, Y., Aras, O., Han, S., Oyama, T., Takeda, S., et al. (2017). The SWI/SNF Protein PBRM1 Restrains VHL-Loss-Driven Clear Cell Renal Cell Carcinoma. Cell Rep. *18*, 2893–2906.
9. Braun, D.A., Ishii, Y., Walsh, A.M., Van Allen, E.M., Wu, C.J., Shukla, S.A., and Choueiri, T.K. (2019). Clinical Validation of PBRM1 Alterations as a Marker of Immune Checkpoint Inhibitor Response in Renal Cell Carcinoma. JAMA Oncol. *5*, 1631–1633.
10. Gao, W., Li, W., Xiao, T., Liu, X.S., and Kaelin, W.G. (2017). Inactivation of the PBRM1 tumor suppressor gene amplifies the HIF-response in VHL-/- clear cell renal carcinoma. Proc. Natl. Acad. Sci. USA *114*, 1027–1032.
11. Varela, I., Tarpey, P., Raine, K., Huang, D., Ong, C.K., Stephens, P., Davies, H., Jones, D., Lin, M.-L., Teague, J., et al. (2011). Exome sequencing identifies frequent mutation of the SWI/SNF complex gene PBRM1 in renal carcinoma. Nature *469*, 539–542.
12. Bratslavsky, G., Gay, L.M., Sokol, E., Elvin, J.A., Vergilio, J.-A., Suh, J., Ramkissoon, S.H., Daniel, S., Severson, E.A., Killian, J.K., et al. (2018). PBRM1 mutation and immunotherapy efficacy: A comprehensive genomic profiling (CGP) assessment. J. Clin. Oncol. *36*, 12091.
13. Jiao, Y., Pawlik, T.M., Anders, R.A., Selaru, F.M., Streppel, M.M., Lucas, D.J., Niknafs, N., Guthrie, V.B., Maitra, A., Argani, P., et al. (2013). Exome sequencing identifies frequent inactivating mutations in BAP1, ARID1A and PBRM1 in intrahepatic cholangiocarcinomas. Nat. Genet. *45*, 1470–1473.
14. Zhou, H., Liu, J., Zhang, Y., Huang, Y., Shen, J., Yang, Y., Fang, W., and Zhang, L. (2020). PBRM1 mutation and preliminary response to immune checkpoint blockade treatment in non-small cell lung cancer. npj Precis. Oncol. *4*, 6.
15. Gu, X., Enane, F., Tohme, R., Schuerger, C., Radivoyevitch, T., Parker, Y., Zuberi, E., Przychodzen, B., Jha, B.K., Lindner, D., et al. (2021). PBRM1 loss in kidney cancer unbalances the proximal tubule master transcription factor hub to repress proximal tubule differentiation. Cell Rep. *36*, 109747.
16. Sinha, S., Biswas, M., Chatterjee, S.S., Kumar, S., and Sengupta, A. (2020). Pbrm1 Steers Mesenchymal Stromal Cell Osteolineage Differentiation by Integrating PBAF-Dependent Chromatin Remodeling and BMP/TGF-β Signaling. Cell Rep. *31*, 107570.
17. Kakarougkas, A., Ismail, A., Chambers, A.L., Riballo, E., Herbert, A.D., Künzel, J., Löbrich, M., Jeggo, P.A., and Downs, J.A. (2014). Requirement for PBAF in Transcriptional Repression and Repair at DNA Breaks in Actively Transcribed Regions of Chromatin. Mol. Cell *55*, 723–732.
18. Indra, A.K., Dupé, V., Bornert, J.-M., Messaddeq, N., Yaniv, M., Mark, M., Chambon, P., and Metzger, D. (2005). Temporally controlled targeted somatic mutagenesis in embryonic surface ectoderm and fetal epidermal keratinocytes unveils two distinct developmental functions of BRG1 in limb morphogenesis and skin barrier formation. Development *132*, 4533–4544.
19. Bao, X., Tang, J., Lopez-Pajares, V., Tao, S., Qu, K., Crabtree, G.R., and Khavari, P.A. (2013). ACTL6a enforces the epidermal progenitor state by suppressing SWI/SNF-dependent induction of KLF4. Cell Stem Cell *12*, 193–203.
20. Chang, C.Y., Shipony, Z., Lin, S.G., Kuo, A., Xiong, X., Loh, K.M., Greenleaf, W.J., and Crabtree, G.R. (2021). Increased ACTL6A occupancy within mSWI/SNF chromatin remodelers drives human squamous cell carcinoma. Mol. Cell *81*, 4964–4978.e8.
21. Saladi, S.V., Ross, K., Karaayvaz, M., Tata, P.R., Mou, H., Rajagopal, J., Ramaswamy, S., and Ellisen, L.W. (2017). ACTL6A Is Co-Amplified with p63 in Squamous Cell Carcinoma to Drive YAP Activation, Regenerative Proliferation, and Poor Prognosis. Cancer Cell *31*, 35–49.
22. Chen, X., Lloyd, S.M., Kweon, J., Gamalong, G.M., and Bao, X. (2021). Epidermal progenitors suppress GRHL3-mediated differentiation through intronic polyadenylation promoted by CPSF-HNRNPA3 collaboration. Nat. Commun. *12*, 448.
23. Lloyd, S.M., Leon, D.B., Brady, M.O., Rodriguez, D., McReynolds, M.P., Kweon, J., Neely, A.E., Blumensaadt, L.A., Ho, P.J., and Bao, X. (2022). CDK9 activity switch associated with AFF1 and HEXIM1 controls differentiation initiation from epidermal progenitors. Nat. Commun. *13*, 4408.
24. Cho, K.F., Branon, T.C., Udeshi, N.D., Myers, S.A., Carr, S.A., and Ting, A.Y. (2020). Proximity labeling in mammalian cells with TurboID and split-TurboID. Nat. Protoc. *15*, 3971–3999.
25. Branon, T.C., Bosch, J.A., Sanchez, A.D., Udeshi, N.D., Svinkina, T., Carr, S.A., Feldman, J.L., Perrimon, N., and Ting, A.Y. (2018). Efficient proximity labeling in living cells and organisms with TurboID. Nat. Biotechnol. *36*, 880–887.
26. He, X., Riceberg, J., Soucy, T., Koenig, E., Minissale, J., Gallery, M., Bernard, H., Yang, X., Liao, H., Rabino, C., et al. (2017). Probing the roles of SUMOylation in cancer cell biology by using a selective SAE inhibitor. Nat. Chem. Biol. *13*, 1164–1171.
27. Battistello, E., Hixon, K.A., Comstock, D.E., Collings, C.K., Chen, X., Rodriguez Hernaez, J., Lee, S., Cervantes, K.S., Hinkley, M.M., Ntatsoulis, K., et al. (2023). Stepwise activities of mSWI/SNF family chromatin remodeling complexes direct T cell activation and exhaustion. Mol. Cell *83*, 1216–1236.e12.
28. Wang, Z., Zhai, W., Richardson, J.A., Olson, E.N., Meneses, J.J., Firpo, M.T., Kang, C., Skarnes, W.C., and Tjian, R. (2004). Polybromo protein

BAF180 functions in mammalian cardiac chamber maturation. Genes Dev. *18*, 3106–3116.

29. Xu, F., Flowers, S., and Moran, E. (2012). Essential role of ARID2 protein-containing SWI/SNF complex in tissue-specific gene expression. J. Biol. Chem. *287*, 5033–5041.
30. Liu, B., Yee, K.M., Tahk, S., Mackie, R., Hsu, C., and Shuai, K. (2014). PIAS1 SUMO ligase regulates the self-renewal and differentiation of hematopoietic stem cells. EMBO J. *33*, 101–113.
31. Liu, B., Tahk, S., Yee, K.M., Fan, G., and Shuai, K. (2010). The ligase PIAS1 restricts natural regulatory T cell differentiation by epigenetic repression. Science *330*, 521–525.
32. Weber, S., Maass, F., Schuemann, M., Krause, E., Suske, G., and Bauer, U.-M. (2009). PRMT1-mediated arginine methylation of PIAS1 regulates STAT1 signaling. Genes Dev. *23*, 118–132.
33. Nishida, T., and Yasuda, H. (2002). PIAS1 and PIASxalpha function as SUMO-E3 ligases toward androgen receptor and repress androgen receptor-dependent transcription. J. Biol. Chem. *277*, 41311–41317.
34. Lindberg, M.J., Popko-Scibor, A.E., Hansson, M.L., and Wallberg, A.E. (2010). SUMO modification regulates the transcriptional activity of MAML1. Faseb. J. *24*, 2396–2404.
35. Kahyo, T., Nishida, T., and Yasuda, H. (2001). Involvement of PIAS1 in the Sumoylation of Tumor Suppressor p53. Mol. Cell *8*, 713–718.
36. Rabellino, A., Melegari, M., Tompkins, V.S., Chen, W., Van Ness, B.G., Teruya-Feldstein, J., Conacci-Sorrell, M., Janz, S., and Scaglioni, P.P. (2016). PIAS1 Promotes Lymphomagenesis through MYC Upregulation. Cell Rep. *15*, 2266–2278.
37. Li, C., McManus, F.P., Plutoni, C., Pascariu, C.M., Nelson, T., Alberici Delsin, L.E., Emery, G., and Thibault, P. (2020). Quantitative SUMO proteomics identifies PIAS1 substrates involved in cell migration and motility. Nat. Commun. *11*, 834.
38. Ouyang, J., Shi, Y., Valin, A., Xuan, Y., and Gill, G. (2009). Direct Binding of CoREST1 to SUMO-2/3 Contributes to Gene-Specific Repression by the LSD1/CoREST1/HDAC Complex. Mol. Cell *34*, 145–154.
39. Yang, S.H., and Sharrocks, A.D. (2004). SUMO promotes HDAC-mediated transcriptional repression. Mol. Cell *13*, 611–617.
40. LeBoeuf, M., Terrell, A., Trivedi, S., Sinha, S., Epstein, J.A., Olson, E.N., Morrisey, E.E., and Millar, S.E. (2010). Hdac1 and Hdac2 act redundantly to control p63 and p53 functions in epidermal progenitor cells. Dev. Cell *19*, 807–818.
41. Neely, A.E., Blumensaadt, L.A., Ho, P.J., Lloyd, S.M., Kweon, J., Ren, Z., and Bao, X. (2023). NUP98 and RAE1 sustain progenitor function through HDAC-dependent chromatin targeting to escape from nucleolar localization. Commun. Biol. *6*, 664.
42. Mashtalir, N., D'avino, A.R., Michel, B.C., Luo, J., Pan, J., Otto, J.E., Zullow, H.J., McKenzie, Z.M., Kubiak, R.L., St Pierre, R., et al. (2018). Modular Organization and Assembly of SWI/SNF Family Chromatin Remodeling Complexes. Cell *175*, 1272–1288.e20.
43. Yao, X., Hong, J.H., Nargund, A.M., Ng, M.S.W., Heng, H.L., Li, Z., Guan, P., Sugiura, M., Chu, P.L., Wang, L.C., et al. (2023). PBRM1-deficient PBAF complexes target aberrant genomic loci to activate the NF-κB pathway in clear cell renal cell carcinoma. Nat. Cell Biol. *25*, 765–777.
44. Sears, R.M., May, D.G., and Roux, K.J. (2019). BioID as a tool for protein-proximity labeling in living cells. Methods Mol. Biol. *2012*, 299–313.
45. Xu, Y., Fan, X., and Hu, Y. (2021). In vivo interactome profiling by enzyme-catalyzed proximity labeling. Cell Biosci. *11*, 27–29.
46. Stewart, S.A., Dykxhoorn, D.M., Palliser, D., Mizuno, H., Yu, E.Y., An, D.S., Sabatini, D.M., Chen, I.S.Y., Hahn, W.C., Sharp, P.A., et al. (2003). Lentivirus-delivered stable gene silencing by RNAi in primary cells. RNA *9*, 493–501.
47. Siprashvili, Z., Nguyen, N.T., Bezchinsky, M.Y., Marinkovich, M.P., Lane, A.T., and Khavari, P.A. (2010). Long-Term Type VII Collagen Restoration to Human Epidermolysis Bullosa Skin Tissue. Hum. Gene Ther. *21*, 1299–1310.
48. Chowdhury, B., Porter, E.G., Stewart, J.C., Ferreira, C.R., Schipma, M.J., and Dykhuizen, E.C. (2016). PBRM1 Regulates the Expression of Genes Involved in Metabolism and Cell Adhesion in Renal Clear Cell Carcinoma. PLoS One *11*, e0153718.
49. Cheng, Z., Gong, Y., Ma, Y., Lu, K., Lu, X., Pierce, L.A., Thompson, R.C., Muller, S., Knapp, S., and Wang, J. (2013). Inhibition of BET Bromodomain Targets Genetically Diverse Glioblastoma. Clin. Cancer Res. *19*, 1748–1759.
50. Ridky, T.W., Chow, J.M., Wong, D.J., and Khavari, P.A. (2010). Invasive three-dimensional organotypic neoplasia from multiple normal human epithelia. Nat. Med. *16*, 1450–1455.
51. Schmittgen, T.D., and Livak, K.J. (2008). Analyzing real-time PCR data by the comparative CT method. Nat. Protoc. *3*, 1101–1108.
52. Ewels, P.A., Peltzer, A., Fillinger, S., Patel, H., Alneberg, J., Wilm, A., Garcia, M.U., Di Tommaso, P., and Nahnsen, S. (2020). The nf-core framework for community-curated bioinformatics pipelines. Nat. Biotechnol. *38*, 276–278.
53. Patro, R., Duggal, G., Love, M.I., Irizarry, R.A., and Kingsford, C. (2017). Salmon provides fast and bias-aware quantification of transcript expression. Nat. Methods *14*, 417–419.
54. Dobin, A., Davis, C.A., Schlesinger, F., Drenkow, J., Zaleski, C., Jha, S., Batut, P., Chaisson, M., and Gingeras, T.R. (2013). STAR: ultrafast universal RNA-seq aligner. Bioinformatics *29*, 15–21.
55. Love, M.I., Huber, W., and Anders, S. (2014). Moderated estimation of fold change and dispersion for RNA-seq data with DESeq2. Genome Biol. *15*, 550–621.
56. Li, H. (2013). Aligning sequence reads, clone sequences and assembly contigs with BWA-MEM. Preprint at arXiv.
57. Heinz, S., Benner, C., Spann, N., Bertolino, E., Lin, Y.C., Laslo, P., Cheng, J.X., Murre, C., Singh, H., and Glass, C.K. (2010). Simple combinations of lineage-determining transcription factors prime cis-regulatory elements required for macrophage and B cell identities. Mol. Cell *38*, 576–589.
58. Kent, W.J., Sugnet, C.W., Furey, T.S., Roskin, K.M., Pringle, T.H., Zahler, A.M., and Haussler, D. (2002). The Human Genome Browser at UCSC. Genome Res. *12*, 996–1006.
59. Quinlan, A.R., and Hall, I.M. (2010). BEDTools: a flexible suite of utilities for comparing genomic features. Bioinformatics *26*, 841–842.
60. Yu, G., Wang, L.G., and He, Q.Y. (2015). ChIPseeker: an R/Bioconductor package for ChIP peak annotation, comparison and visualization. Bioinformatics *31*, 2382–2383.
61. Ross-Innes, C.S., Stark, R., Teschendorff, A.E., Holmes, K.A., Ali, H.R., Dunning, M.J., Brown, G.D., Gojis, O., Ellis, I.O., Green, A.R., et al. (2012). Differential oestrogen receptor binding is associated with clinical outcome in breast cancer. Nature *481*, 389–393.
62. Ramírez, F., Ryan, D.P., Grüning, B., Bhardwaj, V., Kilpert, F., Richter, A.S., Heyne, S., Dündar, F., and Manke, T. (2016). deepTools2: a next generation web server for deep-sequencing data analysis. Nucleic Acids Res. *44*, W160–W165.

STAR★METHODS

KEY RESOURCES TABLE

REAGENT or RESOURCE	SOURCE	IDENTIFIER
Antibodies		
Anti-PBRM1	Bethyl	Cat#A700-019; RRID:AB_2891820
Anti-PIAS1 (D33A7)	Cell Signaling	Cat#3550; RRID:AB_1904090
Anti-PIAS1 (F-1)	Santa Cruz Biotechnology	Cat#sc-365127; RRID:AB_10707973
Anti-ARID2 (D8D8U)	Cell Signaling	Cat#82342; RRID:AB_2799992
Anti-BRG1 (G-7)	Santa Cruz Biotechnology	Cat#sc-17796; RRID:AB_626762
Anti-ARID1A (PSG3)	Santa Cruz Biotechnology	Cat#sc-32761; RRID:AB_673396
Anti-BRD7	Bethyl	Cat#A302-304A-T; RRID:AB_1850214
Anti-BRD7	Bethyl	Cat#A700-221-T
Anti-HA (C29F4)	Cell Signaling	Cat#3724; RRID:AB_1549585
Anti-HA	Proteintech	Cat#66006-2-Ig; RRID:AB_2881490
Anti-Lamin A/C (E−1)	Santa Cruz Biotechnology	Cat#sc-376248; RRID:AB_10991536
Anti-SUMO-1 (D-11)	Santa Cruz Biotechnology	Cat#sc-5308; RRID:AB_628300
Anti-SUMO-2/3/4 (C-3)	Santa Cruz Biotechnology	Cat#sc-393144; RRID:AB_2905545
Anti-COL7A1 (4D2)	Santa Cruz Biotechnology	Cat#sc-33710; RRID:AB_2229746
Mouse IgG (G3A1)	Cell Signaling	Cat#5415; RRID:AB_10829607
IRDye 680LT goat anti-mouse	LI-COR	Cat#926–68020; RRID:AB_10706161
IRDye 800CW goat anti-rabbit	LI-COR	Cat#926–32211; RRID:AB_621843
Goat anti-Mouse IgG (H + L) Alexa Fluor 594	Invitrogen	Cat#A-11005; RRID:AB_2534073
Goat anti-Rabbit IgG (H + L) Alexa Fluor 488	Invitrogen	Cat#A-11034; RRID:AB_2576217
Chemicals, peptides, and recombinant proteins		
ML792	MedChemExpress	Cat#HY-108702
SuperScript VILO Master Mix	Invitrogen	Cat#11755050
PowerUp SYBR Green Master Mix	Applied Biosystems	Cat#A25742
Quick Start Bradford 1x Dye Reagent	Bio-Rad	Cat#5000205
NuPAGE LDS Sample Buffer (4X)	Invitrogen	Cat#NP0008
Dynabeads Protein G	Invitrogen	Cat#10004D
Dynabeads MyOne Streptavidin C1	Invitrogen	Cat#65001
cOmplete, Mini, EDTA-free Protease Inhibitor Cocktail	Roche	Cat#11836170001
16% Formaldehyde	Pierce	Cat#28906
RNase A	Thermo Scientific	Cat#FEREN0531
Proteinase K	Invitrogen	Cat#AM2546
Duolink *In Situ* Detection Reagents Orange	Sigma-Aldrich	Cat#DUO92007
Duolink *In Situ* PLA Probe Anti-Mouse MINUS	Sigma-Aldrich	Cat#DUO92004
Duolink *In Situ* PLA Probe Anti-Rabbit PLUS	Sigma-Aldrich	Cat#DUO92002
Hoechst 33342	Thermo Scientific	Cat#62249
Intercept (PBS) Blocking Buffer	LI-COR	Cat#927-70001
Benzonase Nuclease	Millipore	Cat#E1014-5KU
DBPS	Gibco	Cat#14190144
UltraPure DNase/RNase-Free Distilled Water	Invitrogen	Cat#10977023
Keratinocyte-SFM	Gibco	Cat#17-005-042
Medium 154	Gibco	Cat#M154500
DMEM	Gibco	Cat#11995065
Penicillin-Streptomycin	Gibco	Cat#15140122

(*Continued on next page*)

Continued

REAGENT or RESOURCE	SOURCE	IDENTIFIER
Antibiotic-Antimycotic (100X)	Gibco	Cat#15240062
Fetal Bovine Serum	Cytiva HyClone	Cat#SH3039603HI
TrypLE Express	Gibco	Cat#12604013
Trypsin-EDTA (0.25%)	Gibco	Cat#25200056
Critical commercial assays		
Quick-RNA MiniPrep	Zymo Research	Cat#R1055
ChIP DNA Clean & Concentrator kit	Zymo Research	Cat#D5205
CUTANA ChIC/CUT&RUN Kit	EpiCypher	Cat#14-1048
NEBNext Ultra II DNA Library Prep Kit	NEB	Cat#E7645S
NEBNext Ultra II Directional RNA Library Prep Kit	NEB	Cat#E7760S
NEBNext Poly(A) mRNA Magnetic Isolation Module	NEB	Cat#E7490S
Lipofectamine 3000	Invitrogen	Cat#L3000001
MitoView 633	Biotium	Cat#70055-T
Deposited data		
Raw and analyzed sequencing data	In this paper	GEO: GSE228221
Experimental models: Cell lines		
Primary human keratinocytes	In this paper	N/A
Oligonucleotides		
See Table S7 for oligonucleotides in this study.	In this paper	N/A
Recombinant DNA		
pLKO.1-puro	Addgene	Cat#8453
pCDH-puro-cMyc	Addgene	Cat#46970
TetO-FUW-PBRM1-pgk-puro	Addgene	Cat#85746
3xHA-TurboID-NLS-pCDNA3	Addgene	Cat#107171
pLZRS-3xHA-TurboID-NLS-PBRM1	In this paper	N/A
pLZRS-PBRM1-3xHA-TurboID-NLS	In this paper	N/A
pCDH-HA-PBRM1-puro	In this paper	N/A
pLKO.1-puro-shRNAs targeting PBRM1, PIAS1, BNC1, GTF3C1, NSD3, TASOR, RNF169, CHD1, and PHIP (shRNA sequences listed in Table S7)	In this paper	N/A
Software and algorithms		
GraphPad Prism 9.0	GraphPad Software	RRID: SCR_002798
RStudio	Posit	RRID: SCR_000432
Nextflow		RRID: SCR_024135
Trim Galore		RRID: SCR_011847
FastQC		RRID: SCR_014583
STAR		RRID: SCR_004463
Salmon		RRID: SCR_017036
BWA-MEM		RRID: SCR_010910
MACS2		RRID: SCR_013291
BEDTools		RRID: SCR_006646
HOMER		RRID: SCR_010881
deepTools		RRID: SCR_016366
UCSC Genome Browser		RRID: SCR_005780
DESeq2		RRID: SCR_015687
Diffbind		RRID: SCR_012918
ChIPseeker		RRID: SCR_021322
Scaffold 5	Proteome Software	RRID: SCR_014321
Image Studio	LI-COR	RRID: SCR_015795

(*Continued on next page*)

Continued

REAGENT or RESOURCE	SOURCE	IDENTIFIER
Other		
QuantStudio 3	Applied Biosystems	N/A
Bioruptor Pico	Diagenode	N/A
Odyssey CLx	LI-COR	N/A
Leica CM1860	Leica	N/A
EVOS FL Auto 2	Invitrogen	N/A

RESOURCE AVAILABILITY

Lead contact

Requests for additional information or experimental materials should be directed to Xiaomin Bao (xiaomin.bao@northwestern.edu), the lead contact for this study.

Materials availability

Plasmid constructs or other reagents generated in this study are available upon request. Please contact the lead contact for details.

Data and code availability

All the sequencing data generated in this study, including RNA-seq, ChIP-seq data, and CUT&RUN data, are deposited in GEO (GSE228221). The source data for the figures are deposited in Mendeley (https://doi.org/10.17632/ymsbzh6c7h.1).

EXPERIMENTAL MODEL AND SUBJECT DETAILS

Primary human keratinocyte isolation and culture

Primary human epidermal keratinocytes were isolated from surgically discarded skin specimens. The use of primary keratinocytes in this research has been reviewed by the Institutional Review Board (IRB) at Northwestern University, and it was determined as non-human research. For all the experiments conducted in this study, pre-mixed keratinocytes isolated from 6 de-identified donors were used. These pre-mixed keratinocytes minimize the batch-to-batch variations from different donors, and the next-generation sequencing data could not be identifiable to a specific donor. To culture keratinocytes in the progenitor state, these keratinocytes were cultured in sub-confluent conditions using a 1:1 mixture of Keratinocyte-SFM (Gibco #17-005-142) and Medium 154 (Gibco #M154500). Calcium-induced differentiation was implemented by seeding keratinocytes at 100% confluency with the addition of exogenous 1.2 mM $CaCl_2$ for four days.

METHOD DETAILS

Plasmid construction

All the shRNAs constructs were generated using the pLKO.1-puro vector.[46] The shRNA sequences targeting PBRM1, PIAS1, BNC1, GTF3C1, NSD3, TASOR, RNF169, CHD1, and PHIP were designed using the ThermoFisher BLOCK-iTTM RNAi Designer, and the oligos were synthesized by Integrated DNA Technologies. The shRNA sequences are listed in the Table S7.

All the TurboID constructs were generated using the pLZRS retroviral expression system.[47] The 3xHA-TurboID-NLS sequence was amplified using the 3xHA-TurboID-NLS-pCDNA3 plasmid (Addgene #107171).[25] PBRM1 cDNA sequence was amplified from the TetO-FUW-PBRM1-pgk-puro construct (Addgene #85746).[48] The 3xHA-TurboID-NLS fragment was then added to the N or C terminus of PBRM1 and cloned to the pLZRS vector using In-Fusion (Takara).

The HA-PBRM1 expression plasmid was constructed by adding an HA-tag to the N-terminus of PBRM1, and inserted into the pCDH-puro lentiviral expression vector, modified from the pCDH-puro-cMyc plasmid (Addgene #46970).[49]

Progenitor competition assay in epidermal tissue regeneration

Primary keratinocytes were first labeled with GFP or dsRed using retroviral infection, and subsequently infected with an shRNA targeting genes of interest or non-targeting control shRNA. Equal number (0.5 million) GFP- or DsRed-labelled keratinocytes were mixed and seeded onto a piece of devitalized dermis, and lifted to the liquid-air interface. The tissue was allowed to regenerated for 7 days in organotypic culture.[50] The tissue was then fixed with formalin and embedded with Optimal Cutting Temperature compound (OCT) prior to cryosectioning at 7 uM thickness (Leica). Both red and green fluorescence from the tissue sections were acquired using the EVOS FL Auto Imaging System (Life Technologies).

Gene transfer and expression in keratinocytes

Phoenix and HEK293T cells, cultured in DMEM (Gibco) with 10% fetal bovine serum (HyClone), were used for retroviral or lentiviral mediated gene delivery and expression. For transfection, the Lipofectamine 3000 Transfection Reagent (Invitrogen) was used, following the manufacturer protocol. Viral supernatant was collected 48 h and 72 h after transfection. For the infection, viral supernatant was added to the keratinocytes together with polybrene (20 μg/mL, Sigma) and centrifuged at 1250 rpm for 1 h at 32°C. 24–48 h post infection, the keratinocytes were then selected with puromycin (2 μg/mL, Thermo) for 48 h.

Inhibitor treatments

ML792 (MedChemExpress) was resuspended in DMSO for a working concentration of 10 mM. Keratinocytes were treated with 1 or 5 μM ML792 or equal volumes of DMSO for 24 or 72 h.

Clonogenicity assay

Mouse fibroblast 3T3 cells were treated with mitomycin C (15 μg/mL) in serum-free DMEM for 2 h and then seeded at 8×10^5 cells per well in a 6-well plate. The media was replaced with FAD (Skin Biology and Disease Research Center, Northwestern) the next day and 800 keratinocytes were seeded per well. Over the following 10–12 days, the colony formation was monitored daily with medium changes every other day. At the endpoint, the 3T3 cells were washed away with PBS and the keratinocytes were fixed with 1:1 acetone/methanol for 5 min. The plates were air dried and then stained with crystal violet to visualize the individual clones.

Apoptosis assay

MitoView 633 (Biotium) staining was used to determine potential induction of apoptosis in live keratinocytes. Keratinocytes were seeded onto a 24-well plate. A positive control was included by treating keratinocytes expressing control shRNA with H_2O_2 (2 mM) for 6 h at 37°C. MitoView was added to the keratinocytes at 1:000 and incubated for 20 min in the cell culture incubator. Hoechst 33342 (10 μg/mL, Thermo) was then added for 5 min to stain the DNA before imaging.

Tissue immunofluorescence

Tissue samples were frozen in OCT and cryosectioned at 7 μM thickness (Leica). Each slide was fixed with 10% formalin for 15 min and washed twice with a 1% phosphate-buffered saline (PBS) solution. A solution of 5% goat serum in 1% PBS was applied to each slide for 45 min. A 1:50 ratio of mouse anti-COL7 primary antibody was added to a solution of 1% goat serum in 1% PBS, and split into primary antibody variations, maintaining a 1:200 ratio of anti-rabbit primary antibodies. Each primary antibody mixture was applied to the slides and incubated at 4°C overnight. Primary antibodies used include anti-PBRM1 (Bethyl, A700-019), anti-PIAS1 (D33A7) (Cell Signaling, 3550), and anti-COL7A1 (4D2) (Santa Cruz Biotechnology, sc-33710). The next day, the slides were washed three times with a 1% PBS solution. A 1:400 ratio of Goat anti-Mouse IgG (H + L) Alexa Fluor 594 (Thermo Fisher, A-11005) and a 1:400 ratio of Goat anti-Rabbit IgG (H + L) Alexa Fluor 488 (Thermo Fisher, A-11034) in a 1% goat serum in 1% PBS solution was applied to each slide and incubated at room temperature for 1 h in the dark. After, the slides were washed with 1% PBS, treated with Hoechst 33342 (10 μg/mL, Thermo) for 5 min, and then washed two more times with 1% PBS. Each slide was then mounted and imaged using the EVOS FL Auto 2 imaging system.

RT-qPCR

RNA was extracted using Quick-RNA MiniPrep (Zymo Research) following the manufacturer's protocol. Subsequently, cDNA was synthesized using SuperScript VILO cDNA Master Mix (Invitrogen) following the manufacturer protocol, with equal amount of RNA from control or treated group in each experiment. RT-qPCR was performed using PowerUp SYBR Green Master Mix (Applied Biosystems). The RT-qPCR primers used are listed in the Table S7.

Western blotting

For immunoblot analysis, 10–30 μg of cell lysate was loaded per lane for SDS-page and then transferred to PVDF membranes. Blots were blocked with Odyssey Blocker PBS (Li-COR) + 2.5% BSA at room temperature for 1 h. Blots were then incubated with primary antibody at 4°C overnight and then with secondary antibodies (IRDye 680LT goat anti-mouse, LI-COR, 926–68020, 1:15,000, and/or IRDye 800CW goat anti-rabbit, LI-COR, 926–32211, 1:15,000) at room temperature for 1 h. The blots were imaged using Li-COR Odyssey CLx (LI-COR). Primary antibodies used for western blotting include anti-PBRM1 (Bethyl, A700-019), anti-PIAS1 (D33A7) (Cell Signaling, 3550), anti-ARID2 (D8D8U) (Cell Signaling, 82342), anti-BRG1 (G-7) (Santa Cruz Biotechnology, sc-17796), anti-ARID1A (PSG3) (Santa Cruz Biotechnology, sc-32761), anti-BRD7 (Bethyl, A302-304A-T), anti-HA (C29F4) (Cell Signaling, 3724), and anti-Lamin A/C (E−1) (Santa Cruz Biotechnology, sc-376248).

Co-immunoprecipitation

Nuclei were extracted from keratinocytes using a hypotonic buffer (10 mM HEPES pH 7.5, 1.5 mM $MgCl_2$, 10 mM KCl, 0.2% NP-40, 1× protease inhibitor EDTA free (Roche)). The pelleted nuclei were lysed using IP buffer (50 mM Tris pH 7.5, 150 mM NaCl, 1 mM $MgCl_2$, 5% glycerol, 1% NP-40, 1× protease inhibitor EDTA free (Roche)) with shearing using a 27.5-gauge needle. For immunoprecipitation, anti-HA (Proteintech, 66006-2-Ig), anti-ARID2 (D8D8U) (Cell Signaling, 82342), or Mouse IgG (G3A1) (Cell Signaling, 5415)

antibodies were pre-coupled with Dynabeads Protein G (Invitrogen) overnight at 4°C, and then incubated with the nuclear lysate at 4°C overnight. The next day, the beads were washed with IP wash buffer (150 mM NaCl, 50 mM Tris pH 7.5, 5% glycerol, 0.05% NP-40, 1× protease inhibitor EDTA free (Roche)) 4 times for 10 min each at 4°C. The sample was then eluted with IP wash buffer mixed with loading dye and beta-mercaptoethanol for western blotting.

Proximity ligation assay

Keratinocytes were seeded on Poly-L-ornithine-treated cover slips to culture overnight, and fixed using 10% Buffered Formalin (Fisher Scientific) for 15 min. These coverslips were briefly washed, blocked using blocking buffer (PBS with 0.3% Triton X-100, 3% normal goat serum) and then incubated with anti-HA (C29F4) (Cell Signaling, #3724), anti-SUMO-1 (D-11) (Santa Cruz Biotechnology, sc-5308), or anti-SUMO-2/3/4 (C-3) (Santa Cruz Biotechnology, sc-393144) overnight at 4°C. The next day, cover slips were incubated with PLA probes anti-mouse and anti-rabbit (Sigma-Aldrich). Duolink *In Situ* Detection Reagents Orange (Sigma-Aldrich) was then used for ligation and signal amplification following the manufacturer's protocol. Images were acquired using the EVOS FL Auto 2 imaging system (Thermo Fisher).

PBRM1 TurboID and mass spectrometry

Nuclei were extracted from keratinocytes using a hypotonic buffer (10 mM HEPES pH 7.5, 1.5 mM $MgCl_2$, 10 mM KCL, 0.2% NP-40, 1× protease inhibitor EDTA free (Roche)). The nuclear pellets were subsequently lysed using a lysis buffer (50 mM Tris pH 7.4, 500 mM NaCl, 0.2% SDS, 1 mM DTT, and 2% Triton X-100, 1× protease inhibitor EDTA free (Roche)). The samples were briefly sonicated using the Bioruptor Pico (Diagenode) for 10 cycles of 30 s and 30 s off. A 3 kDa Amicon Ultra-4 Centrifugal Filter Unit (Millipore) was used to remove excess biotin by buffer exchange. The lysate was then incubated with Dynabeads MyOne Streptavidin C1 (Invitrogen) overnight at 4°C. Next day, the beads were washed with wash buffer 1 (2% SDS), wash buffer 2 (50 mM HEPES pH 7.5, 500 mM NaCl, 1% Triton X-100, 1% EDTA, and 10% sodium deoxycholate), and wash buffer 3 (10 mM Tris pH 7.4, 250 mM LiCl, 0.5% NP-40, 0.5% sodium deoxycholate, and 1% EDTA). The samples were eluted with loading dye combined with 20 mM DTT and 4 mM biotin. The eluted samples were loaded onto a polyacrylamide gel, and gel fragments were submitted to the Northwestern Proteomics Core Facility for protein identification using mass spectrometry.

RNA-seq

RNA was extracted using Quick-RNA MiniPrep (Zymo Research) with DNase I treatment following the manufacturer's protocol. RNA-seq libraries were prepared using NEBNext Ultra II Directional RNA Library Prep Kit for Illumina (New England BioLabs) with NEBNext Poly(A) mRNA Magnetic Isolation Module (New England BioLabs). Libraries were sequenced as single-end 50 base pair (bp) reads using the Illumina HiSeq 4000 system at Northwestern University NUSeq Core facility.

ChIP-seq

ChIP-seq was performed as previously described.[5] In brief, approximately 10 million keratinocytes were cross-linked with 1% formaldehyde at room temperature for 10 min. Nuclei was extracted from keratinocytes using a hypotonic buffer and lysed with a RIPA buffer. The lysate was then sonicated using Bioruptor Pico (Diagenode) for 50–200 cycles (30 s on, 30 s off). Antibodies were incubated with Dynabeads Protein G (Invitrogen) and then incubated with nuclei lysate at 4°C overnight. Antibodies used for ChIP-seq include anti-PBRM1 (Bethyl, A700-019) and anti-PIAS1 (F-1) (Santa Cruz, sc-365127). The IP reactions were washed three times sequentially using RIPA buffer with 150 mM NaCl, RIPA buffer with 500 mM NaCl, and RIPA buffer with 500 mM LiCl. Protein-DNA fragments were eluted and reverse crosslinked overnight. Following reverse crosslinking, the samples were treated with Proteinase K and RNase and then purified using the ChIP DNA Clean & Concentrator kit (Zymo).

To prepare ChIP-seq libraries, NEBNext Ultra DNA Library Prep Kit was used following the manufacturer's protocol. Libraries were sequenced as single-end 50 base pair (bp) reads using the Illumina HiSeq 4000 platform at Northwestern University NUSeq Core facility.

CUT&RUN

CUT&RUN was performed using the CUTANA ChIC/CUT&RUN Kit (EpiCypher) following the manufacturer protocol. In brief, ConA beads were activated using Bead Activation Buffer. Half a million keratinocytes were incubated with activated ConA beads for 10 min at room temperature. The supernatant was then removed, and Antibody Buffer was added. Rabbit IgG (provided in the EpiCypher kit) and BRD7 antibody (Bethyl, A700-221-T) was added to the reaction and incubated on the nutator overnight at 4°C. The next day, the reactions were washed twice with cold Cell Permeabilization Buffer. 2.5 μL of pAG-MNase was added to each reaction and incubated for 10 min at room temperature. The reactions were then washed again twice with cold Cell Permeabilization Buffer. 1 μL of 100 mM $CaCl_2$ was added to the reactions and incubated for 2 h at 4°C. After the incubation, a Stop Master Mix consisting of 1 μL E. coli Spike-in DNA and 33 μL Stop Buffer were added to each reaction. The DNA was then purified using the provided DNA purification kit.

NEBNext Ultra II DNA Library Prep Kit was used to prepare CUT&RUN libraries following the manufacturer's protocol. Libraries were sequenced as single-end 50 base pair (bp) reads using the Illumina HiSeq 4000 platform at Northwestern University NUSeq Core facility.

QUANTIFICATION AND STATISTICAL ANALYSIS

Organotypic culture tissue regeneration analysis

The EVOS FL Auto 2 imaging system software (Thermo Fisher) was used to image at least 15 images per condition. Every nucleus with red or green fluorescence were counted along the basal membrane. The ratio of red to green florescence was calculated for each image. The values were visualized using GraphPad Prism where an unpaired t-test was subsequently performed.

Colony formation assay analysis

Colonies greater than 1 mm^2 were counted and averaged across biological replicates. The values were visualized using GraphPad Prism where an unpaired t-test was subsequently performed.

RT-qPCR expression analysis

RT-qPCR data were analyzed using the comparative C_T method.[51] 18S ribosomal RNA was used as the loading control. RT-qPCR data were visualized with GraphPad Prism with the average of the biological replicates with their standard errors. An unpaired t-test was used to determine statistical significance.

RNA-seq data analysis

RNA-seq data raw data was processed using a pipeline constructed using the Nextflow framework.[52] Adaptor trimming and quality control was performed using Trim Galore and FastQC, respectively. Alignment to hg38 reference genome was performed using STAR and transcript quantification was performed using Salmon.[53,54] Differential expression analysis was performed using the R package, DESeq2.[55] Significant genes were filtered using average log 2 (Fold Change) $\geq$ 2, with each individual shRNA log 2 (Fold Change) $\geq$ 1.5, and p value $<$ 0.05.

ChIP-seq and CUT&RUN data analysis

Adaptor trimming and quality control was performed using Trim Galore and FastQC, respectively. Alignment to hg38 reference genome was performed using BWA-MEM.[56] Broad peaks were called using MACS2 with a q-value cutoff of 0.001. Motif analyses were performed using HOMER.[57] Genome browser tracks were visualized using the UCSC Genome Browser.[58] Bigwig files were generated using BEDTools[59] and normalized based on counts per million reads. Peak annotation was performed using the R package, ChIPseeker.[60] Differential analysis was performed using EdgeR via the R package, Diffbind.[61] Significant peaks were filtered using average log 2 (Fold Change) $\geq$ 2 and p value $<$ 0.05. For generating the heatmaps and average profile plots, deepTools[62] was used.

TurboID proteomic data analysis

The proteomics data was visualized using Scaffold. The parameters set were a protein threshold of 1% FDR, minimum number of peptides of 2, and a peptide threshold of 95%. A fold change was calculated by dividing the PBRM1 peptide counts (total of PBRM1-TurboID counts and TurboID-PBRM1 counts) by the control peptide counts. Relative enrichment between the progenitor state (UD) and the differentiation state (DF) was calculated by taking the ratio of the fold change in UD to the fold change of DF.